SLAC-PUB-823
November 1970

K_L^o-p INTERACTIONS FROM 1-8 GeV/c*

A. D. Brody,** W. B. Johnson, B. Kehoe,*** D.W.G.S. Leith,
J.S. Loos, G. J. Luste, K. Moriyasu, B. C. Shen,† W. M. Smart,
F. C. Winkelmann, and R. J. Yamartino

Stanford Linear Accelerator Center
Stanford University, Stanford, California 94305

The preliminary results of the SLAC K_L^o HBC experiment, as presented at the XVth International Conference in High Energy Physics, Kiev, September 1970.

*Work supported by the U. S. Atomic Energy Commission.

**Now at CERN, Geneva.

***On leave from University of Maryland.

†Now at University of California, Riverside.

In this report we give the preliminary results of the SLAC K_L^0 hydrogen bubble chamber experiment as presented to the XVth International High Energy Physics Conference at Kiev. The five separate papers presented at Kiev appear here as sections in the following order:

Section I: Cross Sections for $K_L^0 p$ Interactions from 1 to 8 GeV/c.

Section II: The Reaction $K_L^0 p \rightarrow K_S^0 p$ from 1 to 8 GeV/c.

Section III: The Reaction $\bar{K}^0 p \rightarrow \Lambda \pi^+$ from 1 to 8 GeV/c.

Section IV: Investigation of the $K^{*0} p$ and $K^- \Delta^{++}$ Final States in $K_L^0 p$ Interactions.

Section V: Study of the $K\pi$ Mass Spectrum in the Interval from 1050 to 1250 MeV.

The authors apologize for a few cases of repetition which necessarily occur when the individual papers are grouped together.

We emphasize the preliminary nature of the results contained herein; the experiment is in progress both with regard to higher statistics and refinement of analyses.

I. CROSS SECTIONS FOR $K_L^o p$ INTERACTIONS FROM 1 TO 8 GeV/c

The data presented in this paper come from a 500,000 picture 40" SLAC hydrogen bubble chamber exposure. A special beam line was built for this experment, and its K_L^o and neutron spectra have been measured and reported.[1] The 500 K pictures correspond to a yield of 43 events/μb for K_L^o interactions and this translates to an average of about 30 incident K_L^o's per picture. Figure 1 shows the number of events/μb versus the beam momentum.

The useful range of K_L^o beam momentum is approximately from 1 to 10 GeV/c at the bubble chamber and peaks at 4 GeV/c. A 56-meter flight path from the target to the chamber depletes the low end of the spectrum. The film was exposed under several different beam conditions. Figure 2 illustrates the relative beam spectrum variations over the seven different run conditions. The variations were in the electron energy (10, 16, and 18 GeV/c), its current, the secondary beam production angle (1.6, 2.0, 3.0, and 4.0^o), and the photon absorbers used. Over 80% of the pictures were taken in the runs labeled III, VI, VII in Fig. 2, the three highest yield curves.

One of the unique possibilities in an experiment of this nature is to study distributions as a function of lab momentum (i.e., center-of-mass energy). As all the data points come from the same film sample, the problem of relative systematic errors is not as severe as it could be when comparing different experiments.

We now present our preliminary studies of the cross section variations with beam momentum for the following reactions:

$$K_L^o p \rightarrow K_S^o p \qquad 907 \text{ events} \qquad (1)$$

$$\bar{K}^o p \rightarrow \Lambda \pi^+ \qquad 1026 \text{ events} \qquad (2)$$

and

$$K_L^o p \longrightarrow K_S^o p \pi^+ \pi^- \qquad 3291 \text{ events} \qquad (3)$$

$$\overline{K}^o p \longrightarrow \Lambda \pi^+ \pi^+ \pi^- \qquad 1130 \text{ events} \qquad (4)$$

$$K^o p \longrightarrow K^+ p \pi \qquad 1090 \text{ events} \qquad (5)$$

$$\overline{K}^o p \longrightarrow K^- p \pi \qquad 1720 \text{ events} \qquad (6)$$

The above numbers of events correspond to 35% of the currently available data for the vee topologies and to 10% of the available data for the three pronged topologies.

The absolute cross sections for reactions (1 - 4) have been normalized to the 3 GeV/c $K^- n \longrightarrow \Lambda \pi^-$ point, which has a value of 300 ± 32 μb as determined by the SABRE collaboration.[2] Our data have been corrected for the Λ (or K_S^o) decay escape factor and the losses of slow protons in reaction (1). The error bars for our data in the figures are only statistical and do not reflect any other uncertainties. It should be emphasized that the K_L^o beam spectrum is not as well known below 1.5 GeV/c and above 7 GeV/c as inside this interval. That is, the data points outside this range should have less relative weight.

In Fig. 3 we show our cross sections for reaction (2) and, for comparison, the isospin related cross sections[2] $\sigma(K^- n \longrightarrow \Lambda \pi^-)$ and $2 \times \sigma(K^- p \longrightarrow \Lambda \pi^o)$. The agreement among the cross sections is good over the entire energy interval. The cross section fall-off of $\overline{K}^o p \longrightarrow \Lambda \pi^+$ agrees with the well known p_{LAB}^{-n} law. The hand drawn line has $n = 2.9$ and agrees qualitatively with our data. For similar two body $\overline{K}N$ reaction cross sections, the power-law exponent is quoted as $n = 2.5 \pm 0.5$.[3]

The corresponding data for $K_L^o p \longrightarrow K_S^o p$ are shown in Fig. 4. The $K_S^o p$ final state appears to have nearly the same p_{LAB}^{-n} dependence as $\Lambda \pi^+$. The hand-drawn line in Fig. 4 has $n = 2.6$. However, if only the data points at 3 GeV/c and higher

are used, i.e., outside the s-channel resonance region, the slope is $n \approx 2.0$. This is still higher than the usual slope in ρ Regge pole exchange reactions,[3] as illustrated by

$\pi^- p \rightarrow \pi^0 n$	3 - 18 GeV/c	$n = 1.3 \pm 0.2$
$\pi^+ p \rightarrow \pi^0 \Delta^{++}$	2 - 8 GeV/c	$n = 1.1 \pm 0.2$
$K^- p \rightarrow \overline{K}^0 n$		$n = 1.5 \pm 0.2$

If $K_L^0 p \rightarrow K_S^0 p$ is dominated by ω exchange as suggested by Gilman[4] and if we approximate the intercept of the trajectory at $t = 0$ by $\alpha_\omega(0) \approx 0.5$ and estimate $n \approx 2\alpha(0) - 2$, then one would expect $n \approx 1.0$. However, the observed $n \approx 2.0$ is not inconsistent with other experimental data. The reactions

$$K^- p \rightarrow K^{*0}(890) n$$

$$K^- p \rightarrow K^{*-}(890) p$$

are assumed to be dominated by the π and ω trajectories, respectively, and are found[5] to give $n = 2.0 \pm .4$ and $2.0 \pm .14$ (for the range 2-10 GeV/c in beam momentum). The question of the ω exchange dominance of reaction (1) will be discussed in Section II.

The four-body final states are presented in Figs. 5 through 8.

The cross section variation of $K_L^0 p \rightarrow K_S^0 p\pi^+\pi^-$ is shown in Fig. 5. The low momentum region is dominated by the strong quasi-two-body K*N* final state. In particular the extremely copious S = -1 reaction $\overline{K}^0 p \rightarrow K^{*-} N^{*++}$ is illustrated as the shaded subsample in the $K_S^0 \pi^-$ and $p\pi^+$ mass histograms of Fig. 6. The similar reactions $K^- n \rightarrow K^{*0} N^{*-}$ and $K^+ p \rightarrow K^{*0} N^{*++}$ are known to consume about 50% of the four-body final states between 2.0 and 3.0 GeV/c.[6]

Two other final states in this reaction may prove to be very interesting, namely the diffractive $K_L^0 p \rightarrow Qp$ (and $Q \rightarrow K^*\pi$) off the proton vertex and the nondiffractive $K_L^0 p \rightarrow K_S^0 N^*$ ($N^* \rightarrow p\pi^+\pi^-$) at the K^0 vertex. In both cases it

would be desirable to study the production at a lab momentum where the K*N* final state reflections can be suppressed. However, such a study will require the full statistics of the experiment.

The $\overline{K}^o p \rightarrow \Lambda\pi^+\pi^+\pi^-$ final state cross section shows a more rapid decrease than $K_S^o p\pi^+\pi^-$. Figure 7 has a hand drawn curve (to guide the eye) which falls off as $p_{LAB}^{-1.7}$ from 3 to 8 GeV/c. The data agree well with $K^- n \rightarrow \Lambda\pi^-\pi^-\pi^+$ at 3.0 GeV/c,[2] where the cross section is found to be 530 ± 50 μb (and 180 ± 40 μb for $\Sigma^o\pi^-\pi^-\pi^+$). The $\Lambda\pi^\pm$ mass spectrum in Fig. 8 shows a strong $\Sigma^\pm(1385) \rightarrow \Lambda\pi^\pm$ signal. The $\Sigma^\pm(1385)$ is estimated to be 50% of the $\Lambda\pi^+\pi^+\pi^-$ cross section at 1.8 GeV/c and drops to approximately 30 ± 5% at 4.5 GeV/c. There is a definite enhancement in the $\Lambda\pi$ in the vicinity of 1610 MeV/c^2. However, we cannot presently say whether it is a $Y_1^*(1616)$ resonance[7] or a kinematic contamination of the $\Sigma^o\pi(1660)$ fitted as a Λ event.[8]

The three body final state cross sections of reactions (5) and (6) are shown in Fig 9. A check of our estimate of the K_L^o flux at the bubble chamber is given by our own determination of these cross sections. We have compared absolute normalizations of the cross sections for (5) and (6) to the charge symmetric reactions

$$K^- n \rightarrow \overline{K}^o \pi^- n$$
$$K^+ n \rightarrow K^o \pi^+ n$$

Our preliminary results are 10 ± 10% lower than those for the above reactions at 3.0 GeV/c[(9)] and at 4.5 GeV/c.[10] Therefore we estimate an uncertainty in our spectrum normalization of no more than 15%. Cross sections in Fig. 9 have been raised 10% to have them agree with the charged K data.

The $\overline{K}^o p$ cross section is uniformly higher than $K^o p$ above 2.0 GeV/c. Below 2.0 GeV/c, where s-channel resonances are dominant, the $K^o p$ falls off quickly

but $\overline{K}^{o}p$ does not. The straight lines in Fig. 9 are drawn to guide the eye and have a momentum dependence of $p_{LAB}^{-1.6}$. A more detailed study of these two final states is made in Section IV.

II. THE REACTION $K_L^o p \rightarrow K_S^o p$ FROM 1 TO 8 GeV/c

We report preliminary results of a study of the reaction

$$K_L^o p \rightarrow K_S^o p \qquad (1)$$

in the momentum range from 0.8 to 8.0 GeV/c. This reaction can proceed only via exchange of C = -1, natural spin-parity, charge zero mesons. The possible candidates for such an exchange are the members of the vector nonet — ρ, ω, and ϕ — however, Gilman has shown that in the forward direction the ω is expected to dominate.[4] Away from the forward direction the ρ exchange amplitude is expected to become important. This reaction, therefore, provides a powerful tool in determining the properties of the ω trajectory from the momentum dependent behavior of the differential cross section in the forward direction. Previous attempts at extracting the ω trajectory from

$$\pi N \rightarrow \rho N$$

and

$$\gamma N \rightarrow \pi N$$

have been frustrated by lack of statistics and by the problem of other competing exchanges.[11, 12]

The present experiment has two advantages over previous work: (i) the ω trajectory should be better separated, and (ii) data is available over an extended energy range.

This experiment also provides a measurement of the regeneration phase on hydrogen.

The events from reaction (1) were obtained from an exposure of the SLAC 40" HBC to a K_L^o beam. The details of the beam and the K_L^o momentum spectrum have been described in Section I. The events were found in a scan of 20,000 1-prong + V^o events, were measured on the SLAC NRI film-plane measuring

machines,[13] and processed using TVGP-SQUAW fitting programs. A total of 907 events fit reaction (1); of these fewer than 1% are ambiguous with other hypotheses. Corrections for the loss of events due to scanning inefficiencies for short, steeply-dipping protons, were made as a function of K_L^o momentum. In addition, using the known proper lifetime distribution for K_S^o decay, corrections were made, event by event, for both the very short decay (< 0.5 cm) and for the long (>18 cm) decay losses.

The cross section for reaction (1) as a function of K_L^o laboratory momentum is shown in Fig. 10. The details of the flux normalization are dealt with in Section I. The solid line in Fig. 10 shows the cross section decreasing as $p_{LAB}^{-2.5}$. We mention here that the absolute cross section for p_{LAB} below 1.3 GeV/c may be subject to systematic uncertainties as large as 50% pending a more complete analysis of the K_L^o spectrum at the lowest momentum values. The insert shows the cross section on a linear scale, emphasizing the dominant role of $Y_1^*(1765)$ formation in this reaction at low energies. There is also evidence of structure between 1.5 and 2.0 GeV/c, although detailed examination of this region will require the full statistics of this experiment. The cross section above 2.5 GeV/c, i.e., beyond the resonance region, decreases as p_{LAB}^{-2}, which is characteristic of a large class of meson exchange reactions.[3]

Figure 11 shows the momentum transfer distribution of reaction (1) for four lab momentum intervals: 0.8 - 1.3, 1.3 - 2.0, 2.0 - 4.0, and 4.0 - 8.0 GeV/c. The general features of the distributions are the same in all four energy intervals. There is a steep forward peak, a dip in the region of $|t| = 0.3$ $(GeV/c)^2$, and then a much more gentle decrease of the cross section at large t values.

As shown in the insert of Fig. 10, the momentum interval 0.8 - 1.3 GeV/c appears to be dominated by $Y_1^*(1765)$ formation. The dashed curve in Fig. 11

is the expected differential cross section for a pure $5/2^-$ resonance normalized to the data. We observe that the curve provides a good description of the shape of the differential cross section.

The solid lines in Fig. 11 show the predictions of Blackmon and Goldstein[14] for the momentum transfer distribution at $p_{LAB} \approx 2.6$ GeV/c and ≈ 6.4 GeV/c. Their model assumes this reaction to be dominated by the exchange of ω- and ρ-trajectories, plus ω-pomeron and ρ-pomeron cuts. The parameters for these exchanges are determined from their fits to the reactions

$$K^+p \longrightarrow K^+p$$

and

$$K^-p \longrightarrow K^-p$$

With this choice of parameters, the predicted cross section falls too sharply as a function of t both in the forward direction and beyond the dip at 0.3 $(GeV/c)^2$. The model also disagrees with the observed energy dependence of the forward cross section.

The data above 1.3 GeV/c were used to extract $d\sigma/dt\big|_{t=0}$. The differential cross section for $|t| < 0.3$ $(GeV/c)^2$ was fitted using a maximum likelihood technique to the function

$$\frac{d\sigma}{dt} = \left(\frac{d\sigma}{dt}\right)_0 e^{bt}$$

in each of the energy intervals. Values for the forward cross section and the slope are shown in Table I, and $(d\sigma/dt)_0$ is shown as a function of momentum in Fig. 10. The slopes exhibit substantial shrinkage of the forward differential cross section with increasing beam momentum.

We now evaluate from our data the real and imaginary parts of the forward scattering amplitude from which we can determine the intercept of the ω trajectory and also the phase of the regeneration amplitude in hydrogen. The optical point,

$(d\sigma/dt)_{opt}$, has been calculated at each energy using the relation[15]:

$$\left(\frac{d\sigma}{dt}\right)_{opt} = \frac{1}{64\pi}\left[\sigma_{TOT}(K^+n) - \sigma_{TOT}(K^-n)\right]^2$$

and the calculated values are listed in Table I.

From the measured forward cross section and the above calculated $(d\sigma/dt)_{opt}$ we extract the ratio of the real to imaginary parts and the phase of the forward scattering amplitude:

$$\left|\frac{ReA}{ImA}\right| = \left\{\left(\frac{d\sigma}{dt}\right)_0 \Big/ \left(\frac{d\sigma}{dt}\right)_{opt} - 1\right\}^{1/2}$$

and

$$\phi = \tan^{-1}\left[\frac{ImA}{ReA}\right]$$

The quadrant ambiguity for ϕ may be removed by the optical theorem and Regge theory. Isospin invariance and the optical theorem give:

$$ImA\left(K_L^o p \longrightarrow K_S^o p\right) = \frac{1}{2}\left[ImA(K^+n \longrightarrow K^+n) - ImA(K^-n \longrightarrow K^-n)\right]$$

$$= \frac{k}{8\pi}\left[\sigma_{TOT}(K^+n) - \sigma_{TOT}(K^-n)\right]$$

The experimental values for the total cross sections imply $ImA < 0$. If we assume that ω exchange dominates the forward amplitude, then Regge theory gives the relation:

$$\frac{ReA}{ImA} = \tan\left[\frac{1}{2}\pi\alpha_\omega(0)\right]$$

where α_ω is the trajectory function. For $\alpha_\omega(0)$ between 0 and 1, this relation implies $(ReA/ImA) > 0$. To satisfy these two conditions, ϕ must lie in the third quadrant. The values for $|ReA/ImA|$, ϕ, and $\alpha_\omega(0)$ are given in Table I. The intercept $\alpha_\omega(0)$ is in good agreement with the expected value for an ω trajectory having a slope of 1 $(GeV/c)^{-2}$.

The regeneration phase for hydrogen, ϕ_f, is related to the angle ϕ by

$$\phi_f = \arg\left\{ i\, A\left(K_L^o p \longrightarrow K_S^o p\right)\Big|_{t=0} \right\}$$

$$= \phi + \pi/2$$

Thus we find

$$\phi_f = (-43.4 \pm 4.2)^o.$$

We note that this value agrees well with the experimental value for copper of Bennet et al.,[16] $(-45.2^o \pm 7.3^o)$, with the value for carbon of Bott-Bodenhausen et al.,[17] $(-37^o \pm 10^o)$, and also with the optical model calculation for copper of Bohm et al.,[18] $(-43^o \pm 7^o)$. It would be interesting to determine whether the phase for other regenerator materials are also the same.

In conclusion, we find the main features of the reaction $K_L^o p \longrightarrow K_S^o p$, in the momentum range 0.8 - 8.0 GeV/c, to be the following:

1. The cross section $\sigma\left(K_L^o p \longrightarrow K_S^o p\right)$ falls as p_{LAB}^{-2} for the high energy data;
2. The forward differential cross section $(d\sigma/dt)_0$ falls approximately as p_{LAB}^{-1} for the high energy points;
3. The momentum interval 0.8 - 1.3 GeV/c appears to be dominated by $Y_1^*(1765)$ formation;
4. The magnitudes of the real and imaginary parts of the forward scattering amplitude are approximately equal;
5. The average value of the ω trajectory intercept for the high energy data is 0.48 ± 0.05;
6. The average value of the regeneration phase ϕ_f for the high energy data is $(-43.4 \pm 4.2)^o$.

III. THE REACTION $\bar{K}^o p \rightarrow \Lambda\pi^+$ FROM 1 TO 8 GeV/c

Preliminary results of a study of the reaction

$$\bar{K}^o p \rightarrow \Lambda\pi^+ \qquad (2)$$

are presented, in the momentum range from 0.8 to 8.0 GeV/c. This reaction is of interest at low energies because of the formation of S = -1, I = 1 hyperon resonances in the s-channel. At high energies it is of interest for studies of exchange mechanisms since both the differential cross section and the polarization of the Λ^o provides a powerful test of the various exchange models.

The events for reaction (2) were obtained by scanning, measuring, and fitting procedures identical to those for reaction (1), as described in Section II above. Our present sample consists of 1026 events; of these less than 1% are ambiguous with other hypotheses. Using the known proper lifetime distribution for Λ^o decay, corrections were made, event by event, for both the very short decay (< 0.5cm) and for the long (> 13 cm) decay losses.

The cross section for reaction (2) as a function of K_L^o laboratory momentum is shown in Fig. 12. The details of the flux normalization and cross section calculations are given in Section I above. At present no attempt has been made, beyond kinematic fitting, to remove the $\Sigma^o\pi^+$ contamination from the sample. This contamination is estimated at ($\lesssim$ 10%). The cross section falls as approximately $p_{LAB}^{-2.9}$ over the whole energy range, while the high energy behavior appears less steep. Although this slope is not in good agreement with that expected for S = -1 meson exchange,[3] our cross sections do agree well with the other available data on the related reactions:

$$K^- p \rightarrow \Lambda\pi^o \qquad (2a)$$

and

$$K^- n \rightarrow \Lambda\pi^- \qquad (2b)$$

From isospin invariance we expect

$$\sigma(\bar{K}^0 p \rightarrow \Lambda\pi^+) = \sigma(K^- n \rightarrow \Lambda\pi^-) = 2\sigma(K^- p \rightarrow \Lambda\pi^0).$$

Also shown in Fig. 12, as a solid line, is the prediction of the K*(890), K*(1420) Regge-exchange model of Sarma and Reeder.[19] The prediction is seen to be about a factor of three too small, and does not have the same energy dependence as the data.

In Fig. 13 the momentum transfer distributions for reaction (2) are shown for three momentum intervals: 2-3, 3-5, and 5-8 GeV/c. A general feature is a sharp forward peak which changes slope at about 0.5 GeV^2 at all energies. The forward peak, for $0.1 < |t| < 0.4$ GeV^2, has an exponential slope of 3.3 ± 0.8, 4.8 ± 1.0, and 7.3 ± 1.4 GeV^{-2} for the above three momentum intervals, respectively, showing evidence for shrinkage within the present statistics of this experiment. The values of the slope as a function of center-of-mass energy squared are shown in Fig. 14, together with data from reactions (2a) and (2b), and from the line-reversed reaction[20]

$$\pi^- p \rightarrow \Lambda K^0 \qquad (2c)$$

The differential cross section for these reactions, both in slope and magnitude, should be equal if either the weak or strong forms of K*(890), K*(1420) exchange degeneracy holds.[21] Previous analysis[22] of these reactions indicated a failure of exchange degeneracy. However, as shown in Fig. 14, our highest energy data gives a slope which agrees with the exchange degeneracy predictions. Further evidence of exchange degeneracy is shown in Fig. 15, where the differential cross section for reactions (2) and (2c) are compared. The solid line represents a smooth fit to the data of reaction (2c) at 6 GeV/c; the data points are from this experiment averaged over the momentum interval 5-8 GeV/c. The agreement in slope and magnitude between the two experiments is striking. However, the

presence of $\Sigma^0\pi^+$ contamination in both experiments[23] implies an additional 20-30% uncertainty in the cross sections. Despite these difficulties, the data indicate that exchange degeneracy in reactions (2) and (2c) may be working at high energies (i.e., $\gtrsim$ 6 GeV/c).

In Fig. 16 the differential cross section for reaction (2) is shown averaged over the momentum interval 2-8 GeV/c. The solid line represents the prediction of the Sarma-Reeder model, also averaged over this momentum region. The agreement with the data is poor, both in terms of the absolute cross section and in terms of the structure observed.

The average polarization for the momentum interval 2-8 GeV/c is shown in Fig. 17 together with the Sarma-Reeder prediction. The experimental polarization is large and positive throughout most of the momentum transfer region considered, in agreement with previous observations in reactions (2a) and (2b),[24] and in violent disagreement with the model predictions.

Finally, Fig. 18 shows the center-of-mass π^+ angular distribution for reaction (2), again averaged over the momentum region 2-8 GeV/c. The data show a sharp forward peak, with some structure at $\cos\theta \approx .7$, and a broad dip around $\cos\theta \approx 0$ in agreement with previous experiments.[24] However, at this preliminary stage of the experiment an analysis of the backward scattering region cannot be given.

In conclusion, this preliminary study of the reaction $\overline{K}^0 p \to \Lambda\pi^+$ in the momentum region 2-8 GeV/c has shown:

1. The Sarma-Reeder Regge model for this reaction does not represent the data;
2. The forward differential cross section displays shrinkage as the energy increases;

and

3. The exchange degeneracy between reactions $\overline{K}^{o}p \rightarrow \Lambda\pi^{+}$ and $\pi^{-}p \rightarrow \Lambda K^{o}$ looks promising at high energies in contrast to earlier analysis.

IV. INVESTIGATION OF THE $K^{*0}p$ AND $K^{-}\Delta^{++}$ FINAL STATES IN $K_L^0 p$ INTERACTIONS

A. Introduction

In this section, we present a preliminary analysis of the reactions

$$K^0 p \rightarrow K^+ \pi^- p \tag{5}$$

$$\bar{K}^0 p \rightarrow K^- \pi^+ p \tag{6}$$

with incident momenta from 2.0 to 7.0 GeV/c. We have studied the final states $K^{*0}(890)p$, $\bar{K}^{*0}(890)p$ and $K^-\Delta^{++}(1236)$ and have measured the cross sections as a function of beam momentum. Differential cross sections and decay density matrix elements, averaged over all momenta, are also presented. The cross sections for reactions (5) and (6) as well as the details concerning the K_L^0 beam spectrum are presented in Section I above. The present analysis is based on a sample of data equivalent to ~ 4 events/μb which represents only $\sim$10% of our total available data.

Reactions involving K*N and KΔ final states have been studied at various energies in $K^{\pm}p$ and $K^{\pm}n$ interactions. However, attempts to compare the data with theoretical models over a wide range of energies are complicated by problems of relative normalization and differences in analysis techniques between the various experiments. When more fully analyzed, our experiment will have the advantage of providing data over a wide energy region, nearly free from relative normalization problems and biases resulting from different analyses. In particular, the final states

$$K^0 p \rightarrow K^{*0}(890)p \tag{7}$$

$$\bar{K}^0 p \rightarrow \bar{K}^{*0}(890)p \tag{8}$$

can have no relative normalization uncertainty since they are produced by a K_L^0 beam with equal contributions from both strangeness components.

In Section IV. B we present our results for reactions (7) and (8) and compare them to the Regge model predictions of Dass and Frogatt.[25] In Section IV. C, we present results for the final state

$$\bar{K}^{o}p \rightarrow K^{-}\Delta(1236)^{++} \tag{9}$$

with comparisons to the Regge model predictions of Maor and Krammer,[26] and examine the question of exchange degeneracy in connection with the line-reversed reaction:

$$K^{+}p \rightarrow K^{o}\Delta(1236)^{++} \tag{10}$$

B. K*(890)N Production

Production of K*(890)N has been studied over a wide range of energies in $K^{-}p$,[27] $K^{+}p$,[28] $K^{-}n$,[9,10] and $K^{+}n$[29] collisions. The K*N processes can be separated into charge exchange reactions such as:

$$K^{-}p \rightarrow \bar{K}^{*o}n \tag{11}$$

and

$$K^{+}n \rightarrow K^{*o}p \tag{12}$$

and neutral exchange reactions such as:

$$K^{\pm}p \rightarrow K^{*\pm}p \tag{13}$$

and

$$K^{\pm}n \rightarrow K^{*\pm}n \tag{14}$$

The dominant mechanism for reactions (11) and (12) is unnatural parity exchange (presumably π) whereas the dominant mechanism for (13) and (14) is natural parity exchange. This difference may be understood qualitatively by noting that the isovector amplitudes are suppressed by a factor of 2 in reactions (13) and (14) relative to (11) and (12).

Absorptive peripheral model calculations[30] to K*N data employing π and ω exchange have been successful in describing the decay angular distribution but

not the energy dependence of the cross sections. Recently, Regge model fits by Dass and Froggatt and also by Markytan[31] have provided generally good energy dependent descriptions of existing data. In particular, the model of Dass and Froggatt makes detailed predictions for reactions (7) and (8) (or for the charge symmetric reaction (14)) based upon the parameters found in their fit to data from reactions (11) - (13).

Our results for reactions (7) and (8) are given in Figs. (19 - 21) and in Tables II and III. The curves imposed on the figures are the Dass-Froggatt predictions for reactions (7) and (8).

In Fig. 19 we show the cross sections for (7) and (8) as a function of beam momentum, p_{LAB}. The errors shown are purely statistical; we estimate that systematic uncertainties of our preliminary analysis are less than 15% across the momentum region from 2 to 7 GeV/c. The cross section falls approximately as p_{LAB}^{-2} in good agreement with data from reactions (11) and (12).[32] For comparison, cross section values for the charge symmetric reactions (14) are included and agree well with our results. Note that $\overline{K}^{*o}p$ production is slightly larger than $K^{*o}p$ production in contradiction to the model predictions. The experimental ratio of the integrated cross section from 2 to 7 GeV/c is:

$$R = \frac{\int \sigma(K^{*o}p)\, dp}{\int \sigma(\overline{K}^{*o}p)\, dp} = 0.88 \pm 0.10$$

The model prediction for R is 1.27, which is four standard deviations away from the present experimental ratio.

Figure 20 shows the differential cross sections averaged over the momentum region from 2 GeV/c to 7 GeV/c. The model predictions, also averaged over momentum provide a good description at the present level of statistics.

The density matrix elements for K* decay, evaluated in the Jackson reference frame,[33] are shown in Fig. 21. Because Regge models predict very slow changes of the elements with energy, we have used all events from 2 to 7 GeV/c in determining the density matrix elements. A moment calculation was used and statistical errors only are shown. In agreement with other K*N data, and with the Dass-Froggatt model, unnatural parity exchange (ρ_{00} large) is found to be important only for the smallest $|t|$ region. Our values appear to be fairly well described by the model.

C. $K^-\Delta^{++}$ Production

In Fig. 22 we show the cross section for reaction (9) as a function of beam momentum p_{LAB}. For comparison, we also show the data[34] from reaction (10) and from the reaction[9,10]

$$K^-n \rightarrow \overline{K}^0\Delta^-$$

which is equivalent to reaction (9) by charge independence. We see from Fig. 22 that the K^-n cross sections at 3 and 4.5 GeV/c are consistent with our results for reaction (9). We note further that all three reactions show essentially the same energy dependence p_{LAB}^{-n}, where $n \simeq 1.8$.

The curves shown in Fig. 22 are the predictions of the Regge model calculation of Maor and Krammer for reactions (9) and (10). A comparison of these two reactions provides an important test of the model since the same Regge trajectories, the ρ and A_2, are exchanged in the two reactions. We see that the predicted cross sections correctly fit the data at low energy but do not fall with energy as fast as experiment. The calculation does predict, however, that the K^+p cross sections are larger than the $\overline{K}^0p$ cross sections at all energies, in agreement with the data.

In Figs. 23 and 24 we show the differential cross section $d\sigma/dt$ and the Δ^{++} density matrix elements. Both the model predictions and the experimental

distributions were observed to change very little with energy so we have averaged the data over all incident momenta from 2 to 7 GeV/c in order to increase the statistical accuracy. The general shape of the differential cross section agrees well with the Regge prediction. The density matrix elements are consistent with the predicted values although $\mathrm{Re}\rho_{3,-1}$ may be systematically lower then the predicted curve.

The interesting question of exchange degeneracy of the ρ and A_2 trajectories can also be tested by direct comparison of the two reactions (9) and (10) independently of any model. The hypothesis of "weak" exchange degeneracy predicts that the differential cross sections and therefore, also the total cross sections, should be the same for the two reactions.[21,22] The systematic difference between the cross sections of reactions (9) and (10), seen in Fig. 22 indicates a violation of the "weak" form of exchange degeneracy. As a further investigation of this violation, we show in Table IV a comparison of slopes of the forward differential cross sections for (9) and (10). Within statistical accuracy, there are no obvious differences between the slopes for the two reactions.

V. STUDY OF THE Kπ MASS SPECTRUM IN THE INTERVAL FROM 1050 MeV TO 1250 MeV

We present a preliminary analysis of the Kπ mass spectra from the reactions:

$$K^{o}p \longrightarrow K^{+}\pi^{-}p \qquad (5)$$

$$\overline{K}^{o}p \longrightarrow K^{-}\pi^{+}p \qquad (6)$$

with incident momenta from 3 to 8 GeV/c. The present analysis is based on a data sample equivalent to ~4 events/μb.

In addition to the well known K*(890) and K*(1420) resonances, Kπ mass enhancements have been reported at ~1080 MeV,[35] ~1160 MeV,[36] and ~1260 MeV.[37] The resonance interpretation of any of these peaks is open to question, although Crennel et al.,[36] report a 5 standard deviation peak at 1160 ± 10 MeV with a width of 90 ± 30 MeV in the reaction

$$K^{-}n \longrightarrow \overline{K}^{o}\pi^{-}n \qquad (15)$$

at 3.9 GeV/c. The observed peak is unusual in that most of the events appear to arise through constructive interference with the $\Delta^{-}(1238)$ band.

In Fig. 25 we show our Kπ mass spectrum for reaction (6) summed over the incident momentum interval from 3 to 8 GeV/c. Since reactions (6) and (15) are charge symmetric, and, therefore, may be compared directly, we would expect on the basis of the data of Crennel et al., to observe a peak of about 25 events above background. However, we find no evidence for Kπ enhancement in reaction (6) in the vicinity of 1160 MeV, either inside or outside the $\Delta^{++}(1238)$ band. The solid curve of Fig. 25 is the result of a fit composed of a hand-drawn background (dotted curve) and resonances at 890 and 1420 MeV. A χ^2 value of 18.5 was found for 32 degrees of freedom.

The Kπ mass spectrum for reaction (5), shown in Fig. 26, does exhibit a rather narrow peak at a mass of 1195 ± 15 MeV with a width of 50 ± 25 MeV.

However, at the present time our data do not justify a claim for structure in this mass region. The solid curve represents a fit to the histogram assuming three resonances plus a hand-drawn background (dotted curve) and gives an excellent χ^2 value of 16.1 for 25 degrees of freedom. On the other hand, a fit assuming two resonances (dashed curve) also gives a good χ^2 value of 24.5 for 27 degrees of freedom. Thus, there is a good chance that the observed peak near 1195 MeV may be a statistical fluctuation.

In conclusion, we see no evidence in reaction (6) to support the observation by Crennel et al., of a $K\pi$ enhancement at 1160 MeV. We do see a small peak at $\sim$1195 MeV in the $K\pi$ spectrum of reaction (5), but the present data are also compatible with a statistical fluctuation.

REFERENCES

1. A. D. Brody, W. B. Johnson, D.W.G.S. Leith, G. Loew, G. Luste, R. Miller, K. Moriyasu, B.C. Shen, W. M. Smart, R. Yamartino, Phys. Rev. Letters 22, 966 (1969).
2. K^-n and K^-p references:
   G. F. Cox et al., Nuclear Physics B19, 61 (1970);
   D. Merrill et al., Nuclear Physics B18, 403 (1970);
   W. L. Yen et al., Phys. Rev. 188, 2011 (1969);
   W. Graziano, S. G. Wojcicki, Phys. Rev. 128, 1868 (1962);
   G. W. London et al., Phys. Rev. 143, 1034 (1966);
   M. Hague et al., Phys. Rev. 152, 1148 (1966);
   D. C. Colley et al., Nuovo Cimento L111A, 522 (1968).
3. D.R.O. Morrison, Phys. Letters 22, 528 (1966).
4. F. Gilman, Phys. Rev. 171, 1453 (1968).
5. M. Aderholz et al., Nucl. Phys. B5, 567 (1968).
6. D.R.O. Morrison, Proceedings of the Lund International Conference, (Berlingska Booktryckeriet, 1969); p. 253.
7. D. J. Crennell et al., Phys. Rev. Letters 21, 648 (1968).
8. R. Barloutaud et al., Nucl. Phys. B16, 201 (1970).
9. SABRE Collaboration, Nucl. Phys. B16, 53 (1970).
10. D. D. Carmony et al., Purdue Report No. COO-1428-166 (1970).
11. A. P. Contogouris, J. Tran Thanh Van, and H. J. Lubatti, Phys. Rev. Letters 19, 1352 (1967).
12. V. Barger and L. Durand III, Phys. Rev. Letters 19, 1295 (1967).
13. M. Jensen et al., Report No. SLAC-81, Stanford Linear Accelerator Center (1968).

14. M. L. Blackmon and G. R. Goldstein, Phys. Rev. D1, 2707 (1970).

15. The K^+n and K^-n total cross sections were obtained from:
W. Galbraith et al., Phys. Rev. 138, B913 (1965);
R. L. Cool et al., Phys. Rev. D1, 1887 (1970);
R. J. Abrams et al., Phys. Rev. D1, 1917 (1970).

16. S. Bennett et al., Phys. Letters 29B, 317 (1969).

17. M. Bott-Bodenhausen et al., Proc. Topical Conference on Weak Interactions, CERN Report (1969), p. 329.

18. A. Bohm et al., Phys. Letters 27B, 594 (1968).

19. D. D. Reeder and K.V.L. Sarma, Phys. Rev. 172, 1566 (1968).

20. E. Bertolucci et al., Nuovo Cimento Letters 2, 149 (1969).

21. F. J. Gilman, Phys. Letters 29B, 673 (1969).

22. K. W. Lai and J. Louie, Nucl. Phys. B19, 205 (1970), and references therein.

23. The Λ/Σ^0 ratio in $\pi^-p \longrightarrow K^0(\Lambda/\Sigma^0)$ was estimated in Ref. 20 to be 1.18 ± 0.34 at 6 GeV/c.

24. R. Barloutaud et al., Nucl. Phys. B9, 493 (1969);
D. J. Crennell et al., Phys. Rev. Letters 23, 1347 (1969);
W. L. Yen et al., Phys. Rev. Letters 22, 963 (1969).

25. G. V. Dass and C. D. Froggatt, Nucl. Phys. B19, 611 (1970).

26. M. Krammer and U. Maor, Nuovo Cimento 52A, 308 (1967).

27. K^-p references:
Saclay-Paris-Amsterdam Collaboration, Phys. Letters 12, 352 (1964), (3.0 GeV/c);
J. H. Friedman and R. R. Ross, Phys. Rev. Letters 16, 485 (1966), (2.1, 2.45, 2.64 GeV/c);
F. Schweingruber et al., Phys. Rev. 166, 1317 (1968), (4.1, 5.5 GeV/c);
J. R. Ficenec, H.A. Gordon, W. P. Trower, Phys. Rev. 175, 1725 (1968), (2.7 GeV/c);

Y. W. Kang, Phys. Rev. 176, 1587 (1968), (4.6 GeV/c);
Birmingham-Glasgow-London (I. C.) - Munchen-Oxford-Rutherford Collaboration, Nuovo Cimento 53A, 522 (1968), (6.0 GeV/c);
Aachen-Berlin-CERN-London (I. C.) - Vienna Collaboration, Nucl. Phys. B7, 111 (1968), (10.0 GeV/c).

28. K^+p references:
M. Ferro-Luzzi, R. George, Y. Goldschmidt-Clermont, V. P. Henri, B. Jongejans, D. W. G. S. Leith, G. R. Lynch, F. Miller, and J. M. Perreau, Nuovo Cimento 36, 1101 (1965), (3.0 GeV/c);
CERN-Bruxelles Collaboration, Nuovo Cimento 46, 539 (1966), (3.0, 3.5, 5.0 GeV/c;
CERN-Bruxelles Collaboration, Nuovo Cimento 51A, 401 (1967), (3.5 GeV/c);
Frederick Bomse et al., Phys. Rev. 158, 1281 (1967), (2.26 GeV/c);
Birmingham-Glasgow-Oxford Collaboration, CERN Report 68-7, Vol. 2 (1968), (10 GeV/c);
J. C. Berlinghieri, M. S. Farber, T. Ferbel, B. E. Forman, A. C. Melissinos, P. F. Slattery, H. Yuta, Nucl. Phys. B8, 333 (1968), (13 GeV/c);
V. Gordon Lind, G. Alexander, A. Firestone, C. Fu, and G. Goldhaber, UCRL-1928 (1969), (9.0 GeV/c).

29. CERN-Bruxelles-Munchen Collaboration, Nucl. Phys. B16, 123 (1970).

30. J. D. Jackson, J. T. Donohue, K. Gottfried, R. Keyser, and B. E. Y. Svensson, Phys. Rev. 139, B428 (1965).

31. M. Markytan, Nucl. Phys. B10, 193 (1969).

32. Aachen-Berlin-CERN-London (I. C.) - Vienna Collaboration, Nucl. Phys. B5, 567 (1968).

33. K. Gottfried and J. D. Jackson, Nuovo Cimento 33, 309 (1964).

34. A. Bettini, M. Cresti, S. Limentani, L. Peruzzo, R. Santangelo, D. Locke, D. J. Crennel, W. T. Davies, and P. B. Jones, Phys. Letters 16, 83 (1965); see also Ref. 28.

35. CERN-BRUXELLES Collaboration, Nuovo Cimento 51A, 401 (1967).

36. David J. Crennell, Uri Karshon, Kwan Wu Lai, John S. O'Neall, and J. Michael Scarr, Phys. Rev. Letters 22, 487 (1969).

37. W. P. Dodd, T. Joldersma, R. B. Palmer, and N. P. Samios, Phys. Rev. 177, 1991 (1969).

TABLE I

EXPERIMENTALLY MEASURED PARAMETERS FOR $K_L^o p \rightarrow K_S^o p$

p_{LAB} (GeV/c)	$\left(\frac{d\sigma}{dt}\right)_0$ mb/(GeV/c)^2	$\left(\frac{d\sigma}{dt}\right)_{opt}$ mb/(GeV/c)^2	b (GeV/c)$^{-2}$	$\left\|\frac{ReA}{ImA}\right\|$	ϕ (degrees)	$\alpha_\omega(0)$
1.3 - 2.0	1.71 ± 0.38	0.73 ± 0.02	6.5 ± 2.0	1.15 ± 0.23	-138.4 ± 5.9	0.54 ± 0.07
2.0 - 4.0	0.67 ± 0.12	0.46 ± 0.02	8.7 ± 1.9	0.64 ± 0.23	-123.2 ± 7.9	0.37 ± 0.09
4.0 - 8.0	0.43 ± 0.10	0.21 ± 0.04	10.8 ± 2.3	1.01 ± 0.34	-134.8 ± 9.0	0.50 ± 0.10
Weighted Average	-	-	-	0.92 ± 0.15	-133.4 ± 4.2	0.48 ± 0.05

TABLE II

CROSS SECTIONS

A. Reaction $K^{o}p \rightarrow K^{*o}(890)p$, $K^{*o} \rightarrow K^{+}\pi^{-}$

P Interval GeV/c	Events	Fraction (%)	$\sigma(K^{o}p \rightarrow K^{*o}p)$[a] mb
2 - 3	171	52 ± 6	0.98 ± 0.10
3 - 4	89	33 ± 5	0.38 ± 0.06
4 - 6	62	40 ± 7	0.26 ± 0.05
5 - 7	63	40 ± 7	0.19 ± 0.04

B. Reaction $\overline{K}^{o}p \rightarrow \overline{K}^{*o}(890)p$, $\overline{K}^{*o} \rightarrow K^{-}\pi^{+}$

P Interval	Events	Fraction (%)	$\sigma(\overline{K}^{o}p \rightarrow \overline{K}^{*o}p)$[a] mb
2 - 3	216	41 ± 4	1.18 ± 0.12
3 - 4	113	28 ± 4	0.47 ± 0.06
4 - 5	74	30 ± 5	0.32 ± 0.05
5 - 7	50	26 ± 5	0.16 ± 0.03

C. Reaction $\overline{K}^{o}p \rightarrow K^{-}\Delta^{++}(1236)$

P Interval	Events	Fraction (%)	$\sigma(\overline{K}^{o}p \rightarrow K^{-}\Delta^{++})$ mb
1 - 2	179	60 ± 7	1.68 ± 0.19
2 - 3	225	42 ± 4	0.84 ± 0.08
3 - 4	162	40 ± 4	0.44 ± 0.05
4 - 5	75	31 ± 5	0.21 ± 0.03
5 - 7	61	32 ± 6	0.13 ± 0.03

a. Adjusted to include neutral decay mode.

TABLE III

DENSITY MATRIX ELEMENTS

(Averaged over $2 \leq p \leq 7$ GeV/c)

A. Reaction $K^0 p \rightarrow K^{*0}(890)$; $K^{*0} \rightarrow K^+ \pi^-$

$-t$ (GeV/c)^2	Events	$\rho_{0,0}$	$\rho_{1,-1}$	Re$\rho_{1,0}$
0.00 - 0.10	73	0.50 ± 0.10	0.09 ± 0.07	-0.07 ± 0.05
0.10 - 0.25	82	0.24 ± 0.08	0.26 ± 0.07	-0.02 ± 0.05
0.25 - 0.45	76	0.12 ± 0.07	0.33 ± 0.08	-0.06 ± 0.04
0.45 - 1.00	54	0.03 ± 0.07	0.41 ± 0.08	-0.07 ± 0.05

B. Reaction $\bar{K}^0 p \rightarrow \bar{K}^{*0}(890)p$; $\bar{K}^{*0} \rightarrow K^- \pi^+$

$-t$ (GeV/c)^2	Events	$\rho_{0,0}$	$\rho_{1,-1}$	Re $\rho_{1,0}$
0.00 - 0.10	86	0.40 ± 0.08	0.22 ± 0.07	-0.14 ± 0.04
0.10 - 0.25	114	0.07 ± 0.06	0.24 ± 0.06	-0.06 ± 0.04
0.25 - 0.45	82	0.13 ± 0.07	0.35 ± 0.07	-0.03 ± 0.04
0.45 - 1.00	64	0.03 ± 0.07	0.11 ± 0.09	-0.04 ± 0.05

C. Reaction $\bar{K}^0 p \rightarrow K^- \Delta(1236)^{++}$

$-t$ (GeV/c)^2	Events	$\rho_{3,3}$	Re$\rho_{3,-1}$	Re$\rho_{3,1}$
0.00 - 0.10	76	0.19 ± 0.07	0.12 ± 0.06	-0.14 ± 0.06
0.10 - 0.20	98	0.28 ± 0.06	0.08 ± 0.06	-0.07 ± 0.05
0.20 - 0.40	106	0.27 ± 0.05	0.14 ± 0.05	-0.06 ± 0.05
0.40 - 1.00	102	0.34 ± 0.05	0.10 ± 0.06	-0.07 ± 0.05

TABLE IV

SLOPES OF FORWARD PEAK FOR KN $\longrightarrow$ KΔ

$\bar{K}^o p \longrightarrow \Delta^{++} K^-$		$K^+ p \longrightarrow \Delta^{++} K^o$	
P(GeV/c)	A(GeV/c)$^{-2}$	P(GeV/c)	A(GeV/c)$^{-2}$
2 - 3	2.7 ± 0.5	3.0	3.2 ± 0.6
3 - 4	4.4 ± 0.7	3.5	3.5 ± 0.5
4 - 7	2.7 ± 0.7	5.0	4.1 ± 0.7
		9.0	4.2 ± 0.5

FIGURE CAPTIONS

1. K_L^o beam μb equivalent as a function of momentum for 500 K pictures. The integrated total is 42.5 events/μb.
2. Relative K_L^o beam spectra for different beam conditions. Curves III and VI apply to more than 75% of our present event sample.
3. Cross sections versus laboratory momentum for $\bar{K}^o p \rightarrow \Lambda\pi^+$. The sources for the $K^- p \rightarrow \Lambda\pi^o$ and $K^- n \rightarrow \Lambda\pi^-$ are listed in Ref. 2. The SLAC cross sections are normalized to 300 μb at 3.0 GeV/c as observed by SABRE in $K^- n \rightarrow \Lambda\pi^-$. The straight line represents $p^{-2.9}$ and is drawn to guide the eye. All the SLAC data error bars only represent statistical uncertainty.
4. Cross sections versus laboratory momentum for $K_L^o p \rightarrow K_S^o p$. The cross section is normalized to the $\Lambda\pi^+$ events. The straight line is meant to guide the eye only and corresponds to $p^{-2.6}$.
5. Cross sections versus laboratory momentum for $K_L^o p \rightarrow K_S^o p\pi^+\pi^-$. The cross section is normalized to the $\Lambda\pi^+$ final state events.
6. Mass histograms for $K_S^o\pi^-$ and $p\pi^+$ combinations. The shaded events represent $840 \leq K_S^o\pi^- \leq 940$ MeV and $1150 \leq p\pi^+ \leq 1340$ MeV. About 30% of the events fall in the narrow $\bar{K}^*(890)$, $\Delta^{++}(1238)$ overlap band.
7. Cross sections versus laboratory momentum for $\bar{K}^o p \rightarrow \Lambda\pi^+\pi^-\pi^+$ and for $\bar{K}^o p \rightarrow \Sigma^{\pm}(1385)\pi^{\mp}\pi^+$.
8. Mass histogram of $\Lambda\pi^{\pm}$ in the reaction $\bar{K}^o p \rightarrow \Lambda\pi^+\pi^-\pi^+$. Each event is plotted three times.
9. Cross sections versus laboratory momentum for $\bar{K}^o p \rightarrow K^-\pi^+ p$ and $K^o p \rightarrow K^+\pi^- p$. The SLAC data has been normalized to the charge symmetric reactions $K^- n \rightarrow \bar{K}^o\pi^- n$ and $K^+ n \rightarrow K^o\pi^+ n$ at 3.0 and 4.5 GeV/c.
10. Cross sections and $d\sigma/dt$ (t=0) vs K_L^o momentum for $K_L^o p \rightarrow K_S^o p$.

11. Momentum transfer distributions for $K_L^o p \rightarrow K_S^o p$ for the K_L^o momentum intervals .8 - 1.3, 1.3 - 2, 2 - 4, and 4 - 8 GeV/c. Solid lines are the predictions of Blackmon and Goldstein at 2.6 GeV/c (upper curve) and 6.4 GeV/c (lower curve). The dashed line is the prediction for a $5/2^-$ $Y_1^*(1765)$ resonance.

12. Cross sections versus $\overline{K}^o$ momentum for $\overline{K}^o p \rightarrow \Lambda\pi^+$. The curve is the prediction of the Sarma-Reeder model.

13. $d\sigma/dt(\overline{K}^o p \rightarrow \Lambda\pi^+)$ for $\overline{K}^o$ momentum intervals 2 - 3, 3 - 5, and 5 - 8 GeV/c.

14. Exponential slopes of the forward differential cross sections for two sets of hypercharge-exchange reactions related by π-K line reversal.

15. $d\sigma/dt(\overline{K}^o p \rightarrow \Lambda\pi^+)$ averaged over the $\overline{K}^o$ momentum interval 5 - 8 GeV/c. The curve is a smooth fit to the $\pi^- p \rightarrow K^o(\Lambda/\Sigma^o)$ momentum transfer distribution at 6 GeV/c (Ref. 20).

16. $d\sigma/dt(\overline{K}^o p \rightarrow \Lambda\pi^+)$ averaged over the $\overline{K}^o$ momentum interval 2 - 8 GeV/c. The curve is the prediction of the Sarma-Reeder model.

17. Λ polarization in $\overline{K}^o p \rightarrow \Lambda\pi^+$ averaged over the $\overline{K}^o$ momentum interval 2 - 8 GeV/c. The curve is the prediction of the Sarma-Reeder model.

18. π^+ center-of-mass production angle for $\overline{K}^o p \rightarrow \Lambda\pi^+$ averaged over the $\overline{K}^o$ momentum interval 2 - 8 GeV/c.

19. Cross sections for K*N production versus laboratory momentum. The solid (dashed) curve is the prediction of the Dass-Froggatt model for $K^{*o}p(\overline{K}^{*o}p)$ production in this and the next two figures.

20. Differential cross section for $K^{*o}p$ and $\overline{K}^{*o}p$ production averaged over the laboratory momentum interval from 2 GeV/c to 7 GeV/c.

21. Density matrix elements for K* averaged over the laboratory momentum interval from 2 GeV/c to 7 GeV/c.

22. Cross sections for KΔ production versus laboratory momentum. The solid (dashed) curve is the prediction of the Krammer-Maor model for $K^-\Delta^{++}(K^o\Delta^{++})$ production in this and the next two figures.

23. Differential cross sections for $K^- \Delta^{++}$ production averaged over the laboratory momentum interval from 2 GeV/c to 7 GeV/c.

24. Density matrix elements for Δ^{++} averaged over the laboratory momentum interval from 2 GeV/c to 7 GeV/c.

25. The $K\pi$ mass spectrum for $\overline{K}^0 p \longrightarrow K^- \pi^+ p$ over the incident momentum interval from 3 to 8 GeV/c. The shaded events are from the $\Delta^{++}(1238)$ region. The solid curve is a fit to two resonances plus a hand-drawn background (dotted curve).

26. The $K\pi$ mass spectrum for $K^0 p \longrightarrow K^+ \pi^- p$ over the incident momentum interval from 3 to 8 GeV/c. The solid curve is a fit to three resonances plus a hand-drawn background (dotted curve). The dashed curve is a similar fit to two resonances only.

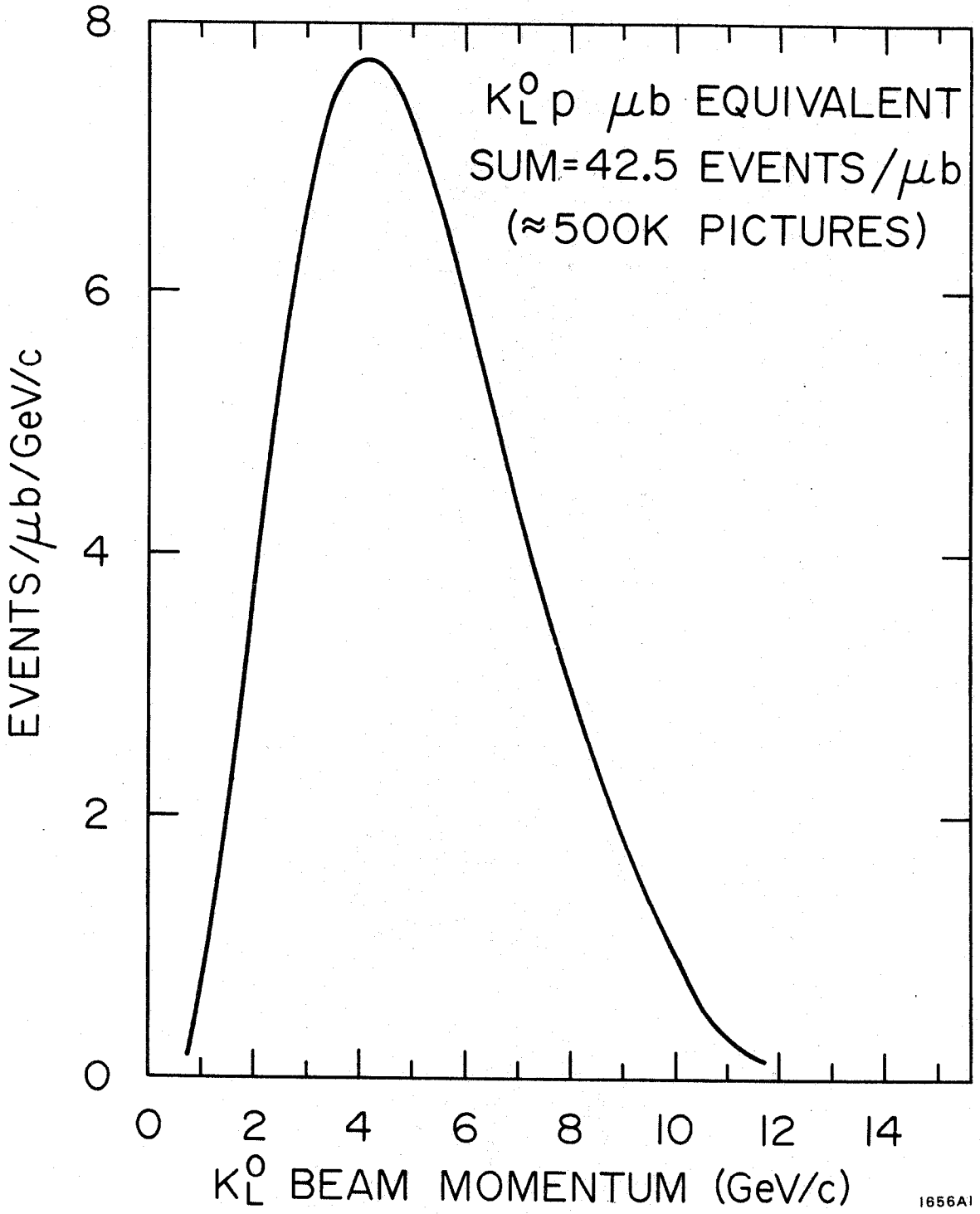
$K_L^0 p$ μb EQUIVALENT
SUM=42.5 EVENTS/μb
(≈500K PICTURES)
EVENTS/μb/GeV/c
0
2
4
6
8
0
2
4
6
8
10
12
14
K_L^0 BEAM MOMENTUM (GeV/c)
1656A1

Fig. 1

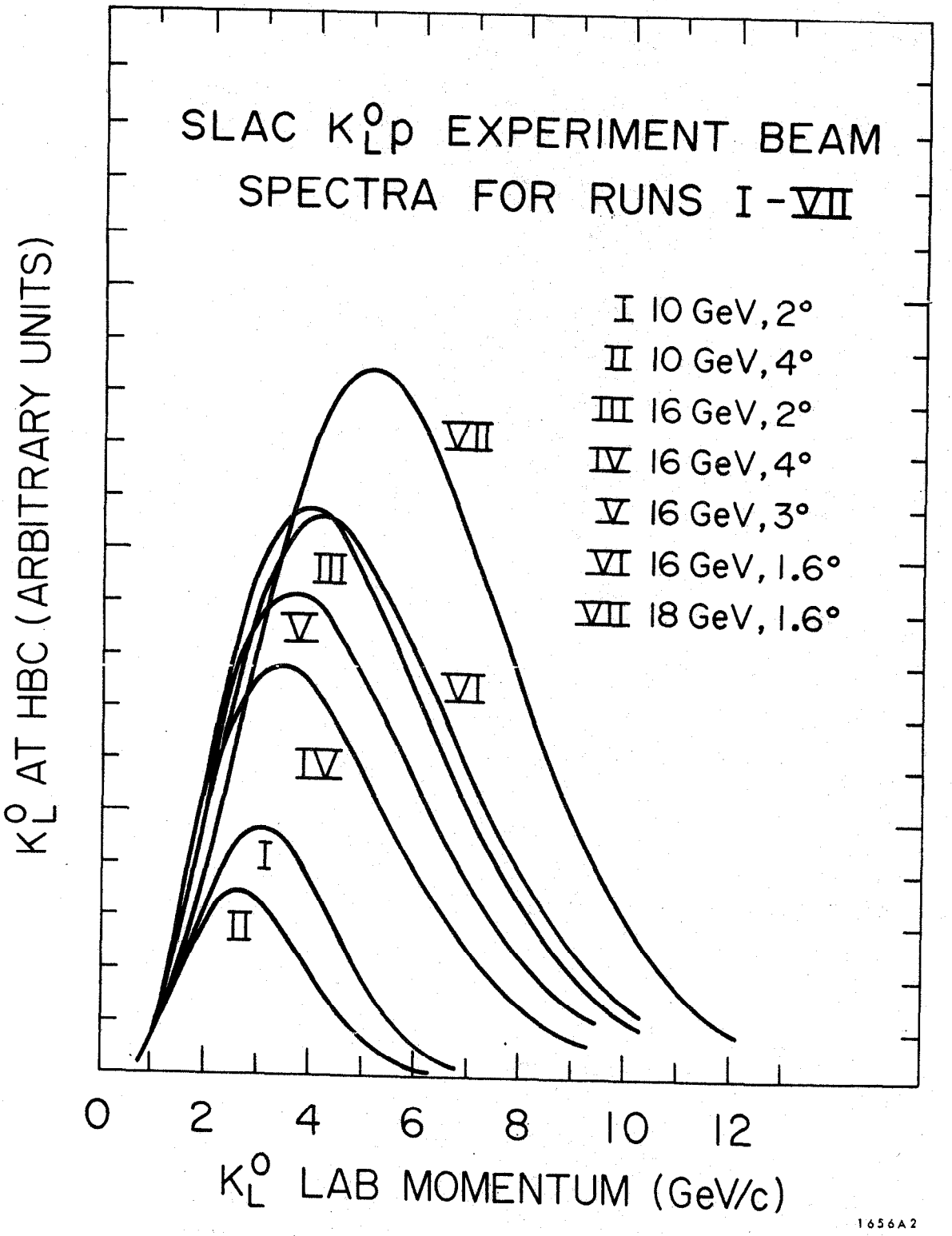
SLAC $K^0_L p$ EXPERIMENT BEAM
SPECTRA FOR RUNS I - VII
I 10 GeV, 2°
II 10 GeV, 4°
III 16 GeV, 2°
IV 16 GeV, 4°
V 16 GeV, 3°
VI 16 GeV, 1.6°
VII 18 GeV, 1.6°
K^0_L AT HBC (ARBITRARY UNITS)
0
2
4
6
8
10
12
K^0_L LAB MOMENTUM (GeV/c)
1656A2

Fig. 2

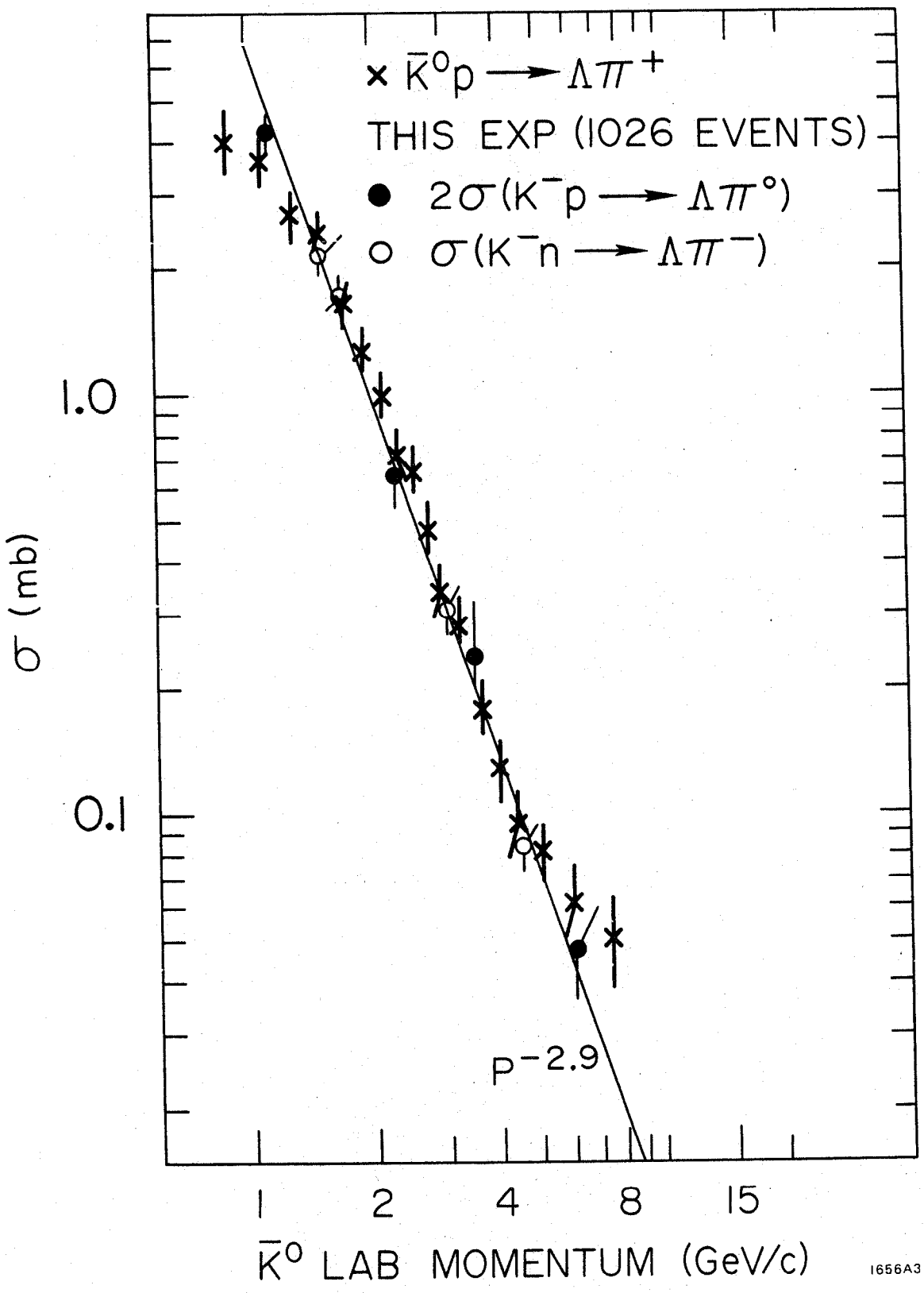
× $\bar{K}^0 p \rightarrow \Lambda\pi^+$
THIS EXP (1026 EVENTS)
● $2\sigma(K^- p \rightarrow \Lambda\pi^0)$
○ $\sigma(K^- n \rightarrow \Lambda\pi^-)$
1.0
0.1
σ (mb)
$p^{-2.9}$
1
2
4
8
15
$\bar{K}^0$ LAB MOMENTUM (GeV/c)
1656A3

Fig. 3

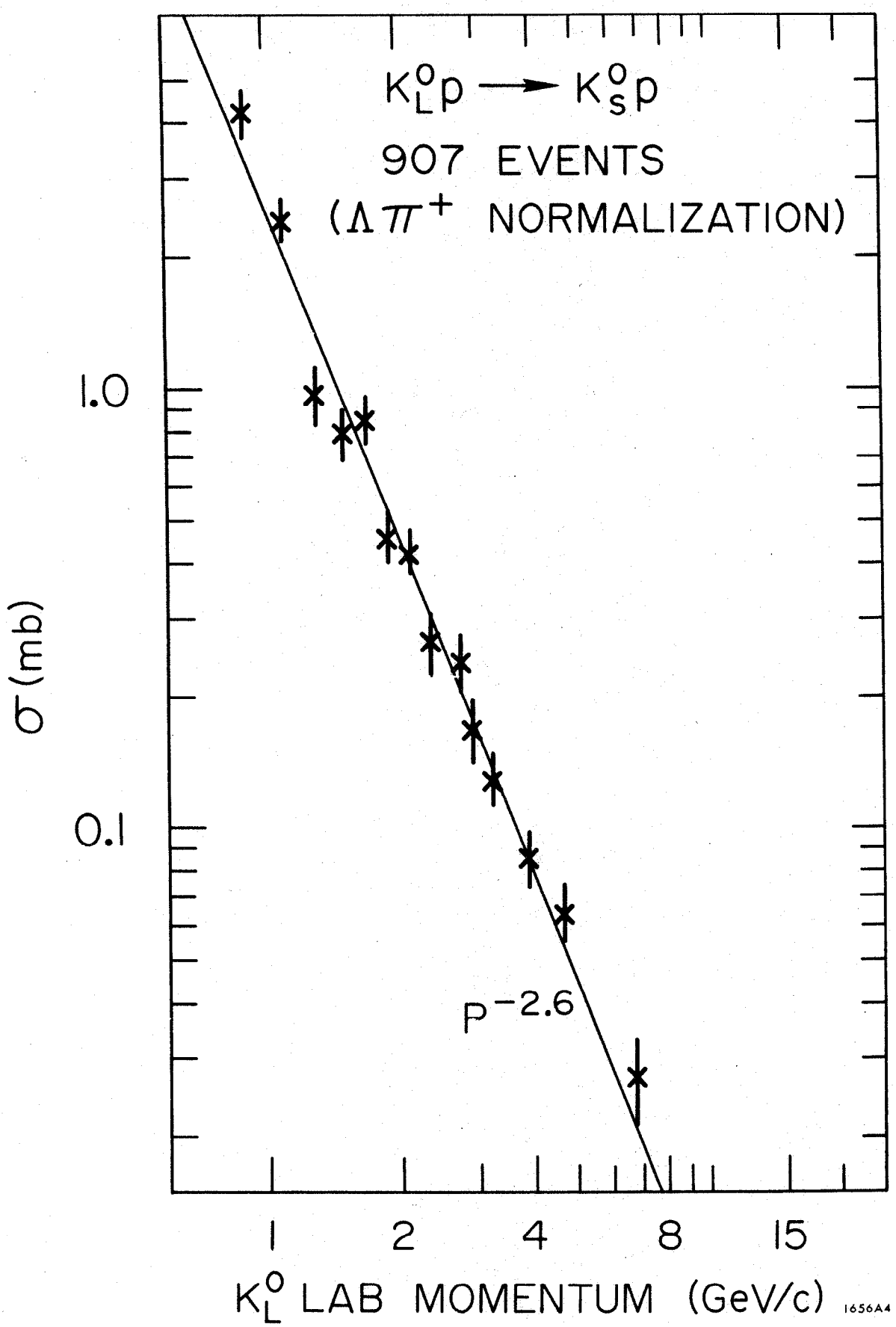
$K_L^0 p \rightarrow K_S^0 p$
907 EVENTS
($\Lambda\pi^+$ NORMALIZATION)
$P^{-2.6}$
1.0
0.1
σ (mb)
1
2
4
8
15
K_L^0 LAB MOMENTUM (GeV/c)
1656A4

Fig. 4

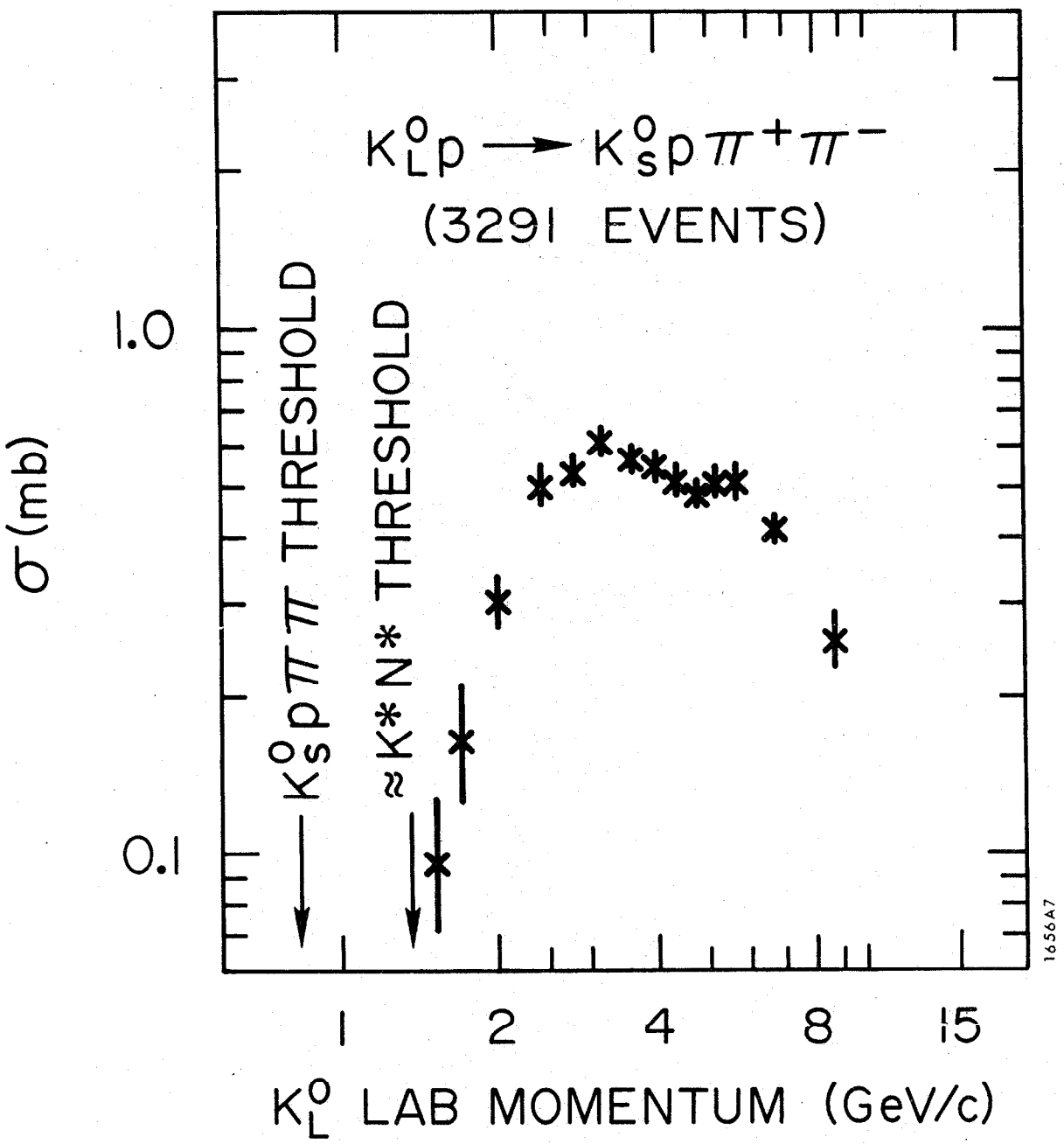
$K^0_L p \rightarrow K^0_S p \pi^+ \pi^-$
(3291 EVENTS)
$K^0_S p \pi \pi$ THRESHOLD
$\approx K^* N^*$ THRESHOLD
1.0
0.1
σ (mb)
1
2
4
8
15
K^0_L LAB MOMENTUM (GeV/c)
1656A7

Fig. 5

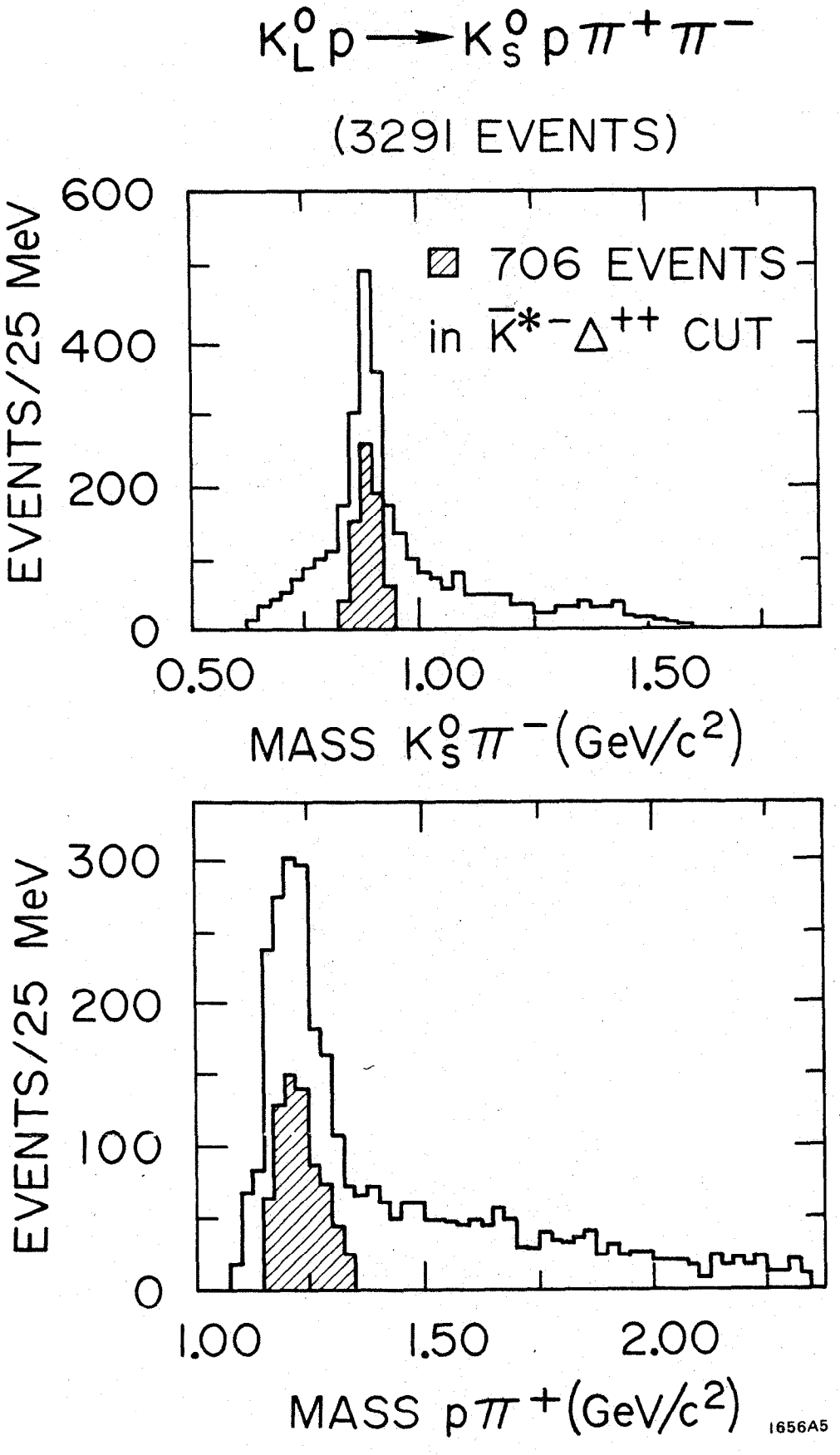
$K_L^0 p \rightarrow K_S^0 p \pi^+ \pi^-$
(3291 EVENTS)
706 EVENTS
in $\bar{K}^{*-}\Delta^{++}$ CUT
EVENTS/25 MeV
600
400
200
0
0.50
1.00
1.50
MASS $K_S^0 \pi^-$ (GeV/c^2)
EVENTS/25 MeV
300
200
100
0
1.00
1.50
2.00
MASS $p\pi^+$ (GeV/c^2)
1656A5

Fig. 6

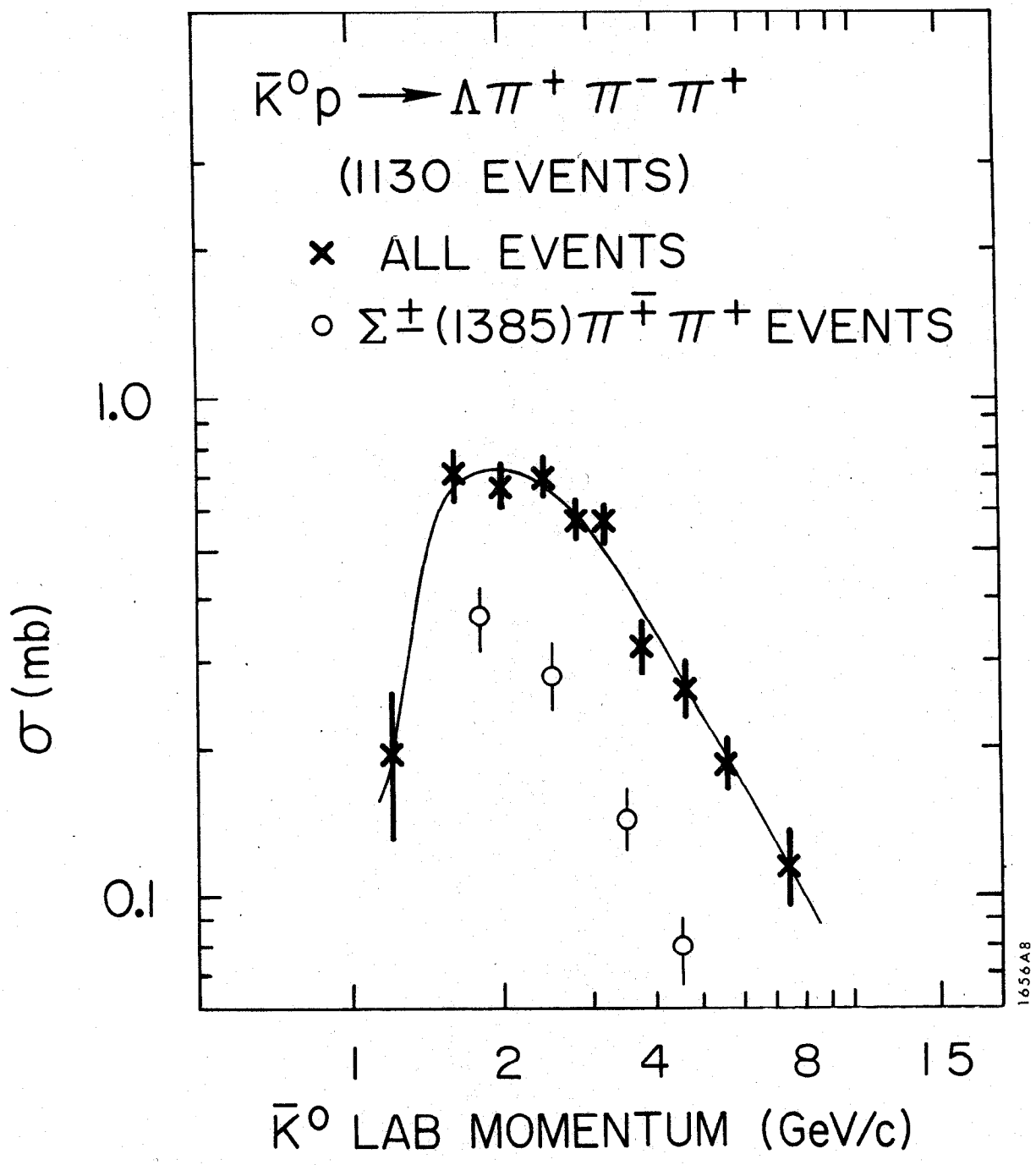
$\bar{K}^0 p \rightarrow \Lambda \pi^+ \pi^- \pi^+$
(1130 EVENTS)
× ALL EVENTS
○ $\Sigma^{\pm}(1385)\pi^{\mp}\pi^+$ EVENTS
1.0
0.1
σ (mb)
1
2
4
8
15
$\bar{K}^0$ LAB MOMENTUM (GeV/c)
1656A8

Fig. 7

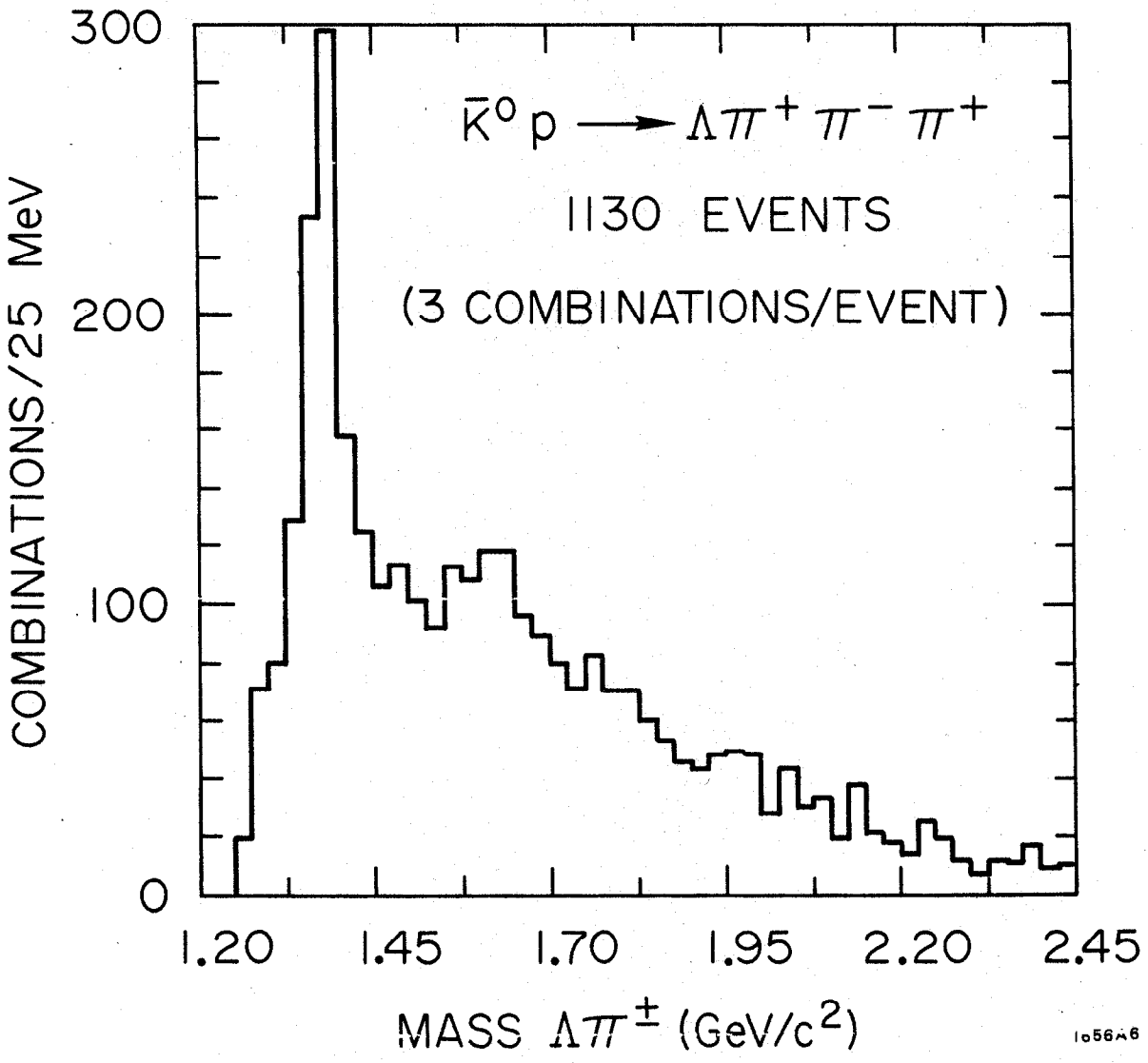
300
200
100
0
COMBINATIONS/25 MeV
$\bar{K}^0 p \longrightarrow \Lambda\pi^+\pi^-\pi^+$
1130 EVENTS
(3 COMBINATIONS/EVENT)
1.20
1.45
1.70
1.95
2.20
2.45
MASS $\Lambda\pi^\pm$ (GeV/c^2)
1056A6

Fig. 8

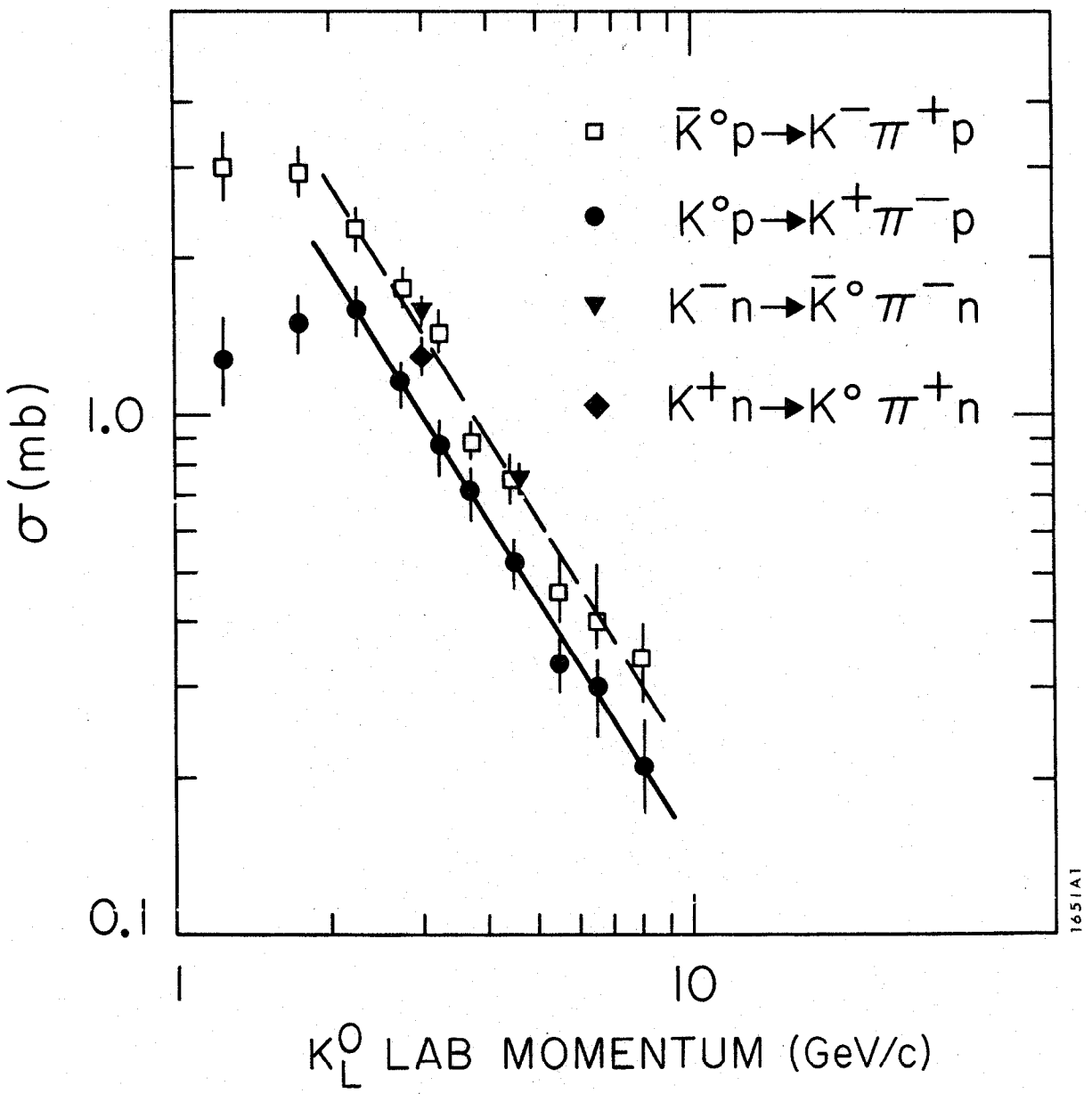
$\bar{K}^0 p \to K^- \pi^+ p$
$K^0 p \to K^+ \pi^- p$
$K^- n \to \bar{K}^0 \pi^- n$
$K^+ n \to K^0 \pi^+ n$
σ (mb)
1.0
0.1
1
10
K^0_L LAB MOMENTUM (GeV/c)
1651A1

Fig. 9

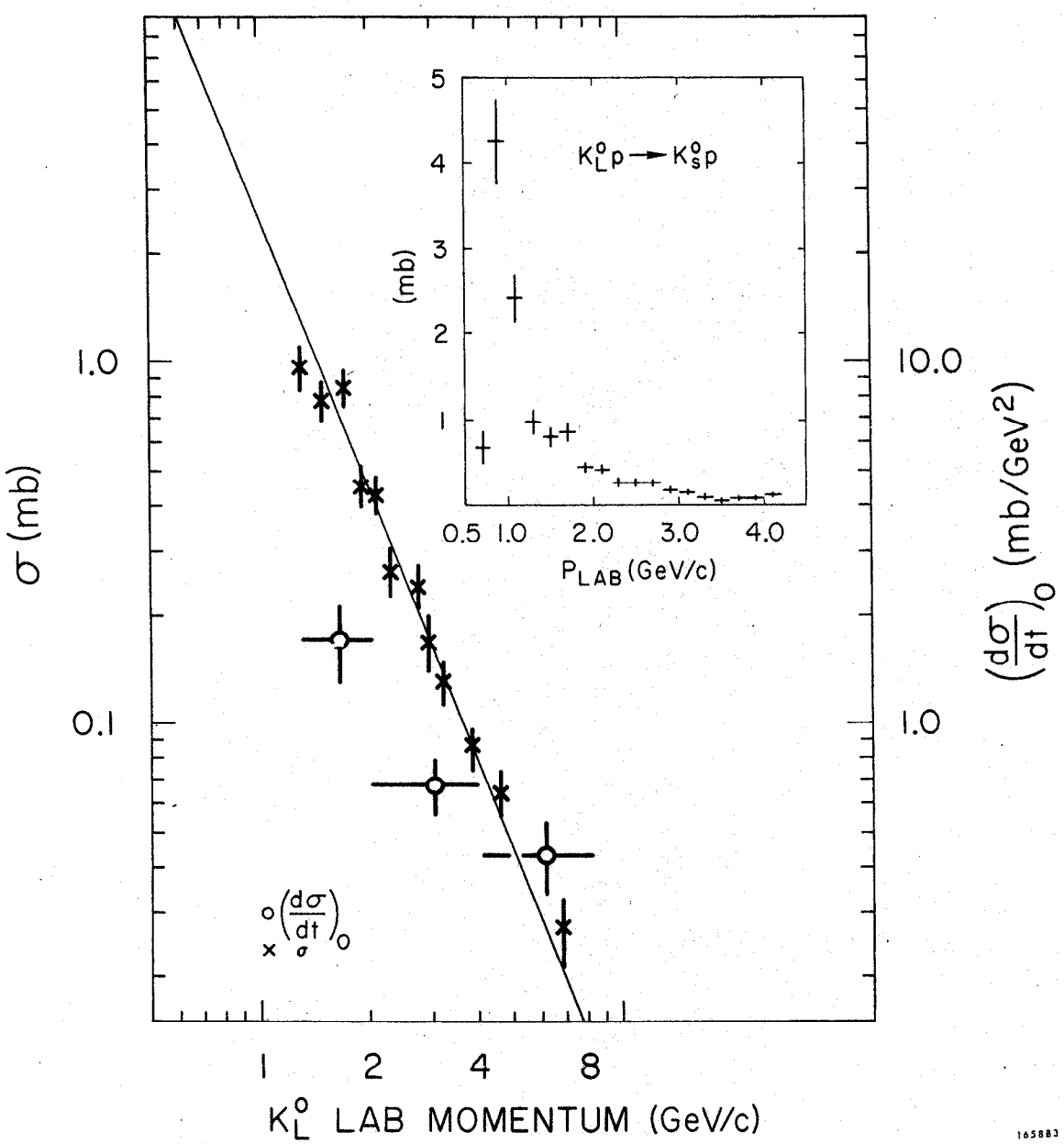
σ (mb)
1.0
0.1
10.0
1.0
(dσ/dt)₀ (mb/GeV²)
1
2
4
8
K⁰L LAB MOMENTUM (GeV/c)
K⁰L p → K⁰S p
(mb)
5
4
3
2
1
0.5 1.0 2.0 3.0 4.0
PLAB (GeV/c)
o (dσ/dt)₀
× σ
165883

Fig. 10

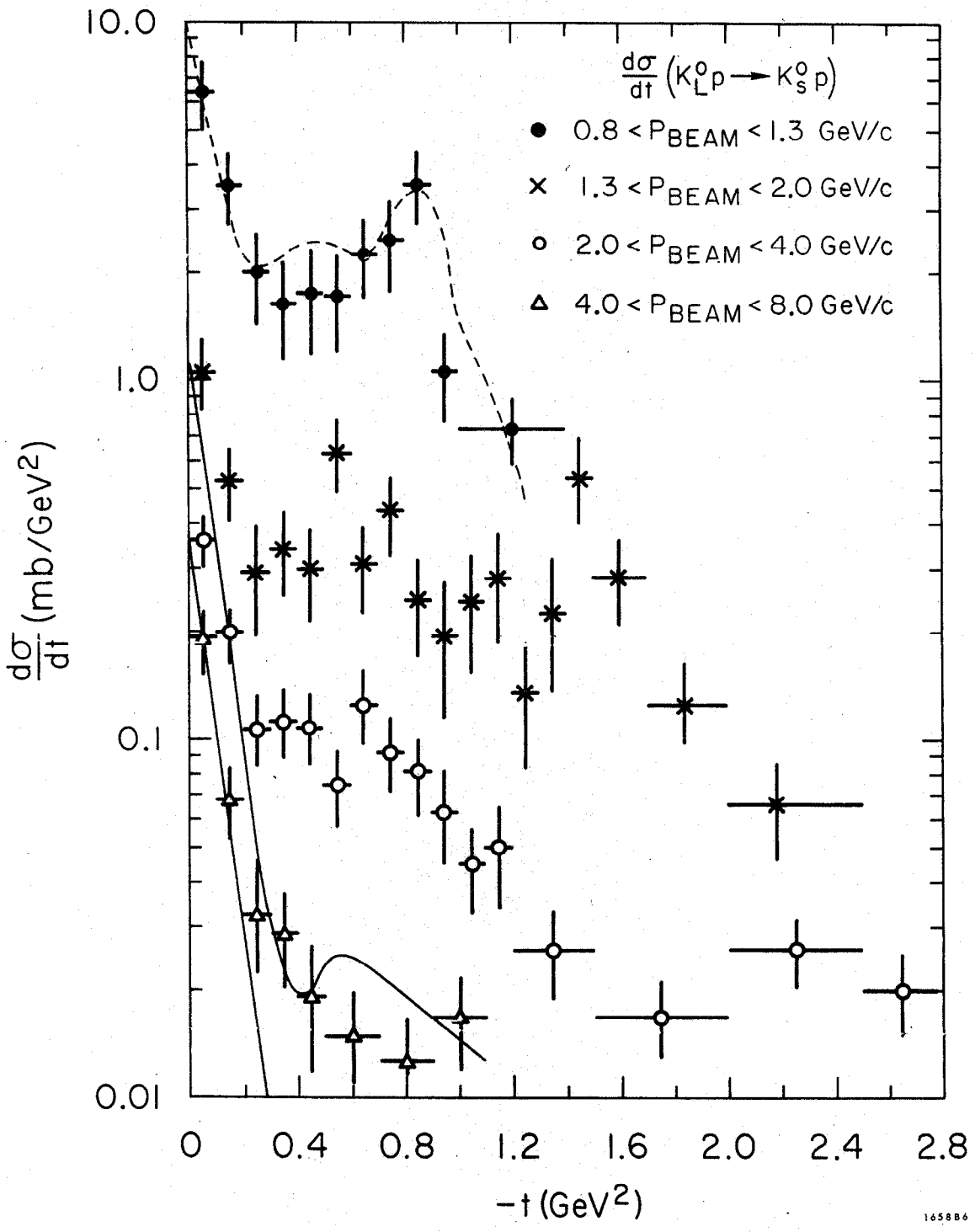
10.0
1.0
0.1
0.01
$\frac{d\sigma}{dt}$ (mb/GeV^2)
$\frac{d\sigma}{dt}(K^0_L p \rightarrow K^0_S p)$
● 0.8 < P_{BEAM} < 1.3 GeV/c
× 1.3 < P_{BEAM} < 2.0 GeV/c
○ 2.0 < P_{BEAM} < 4.0 GeV/c
△ 4.0 < P_{BEAM} < 8.0 GeV/c
0
0.4
0.8
1.2
1.6
2.0
2.4
2.8
$-t$ (GeV^2)
1658B6

Fig. 11

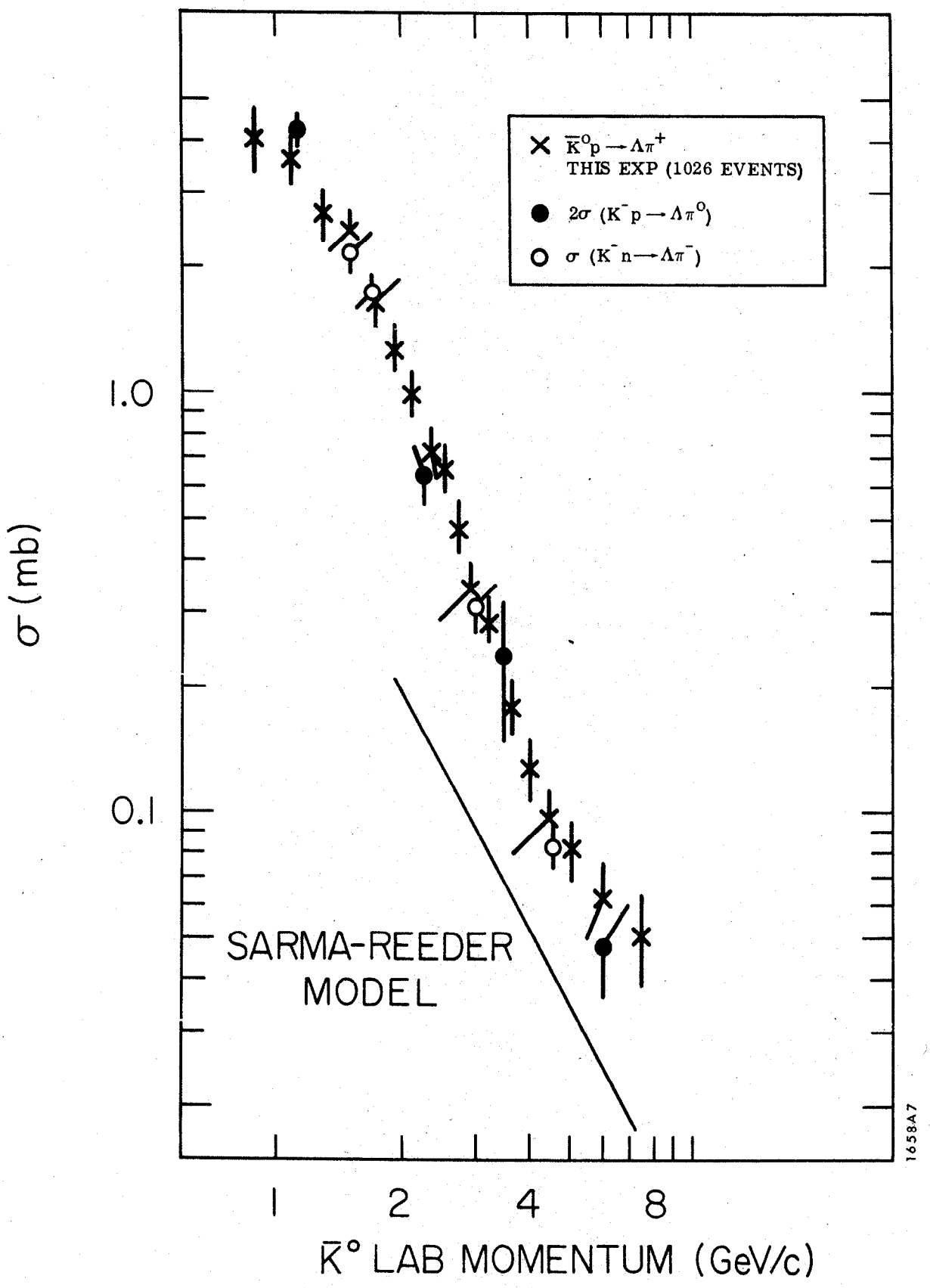
$\bar{K}^0 p \rightarrow \Lambda\pi^+$
THIS EXP (1026 EVENTS)
2σ ($K^- p \rightarrow \Lambda\pi^0$)
σ ($K^- n \rightarrow \Lambda\pi^-$)
1.0
0.1
σ (mb)
SARMA-REEDER
MODEL
1
2
4
8
$\bar{K}^0$ LAB MOMENTUM (GeV/c)
1658A7

Fig. 12

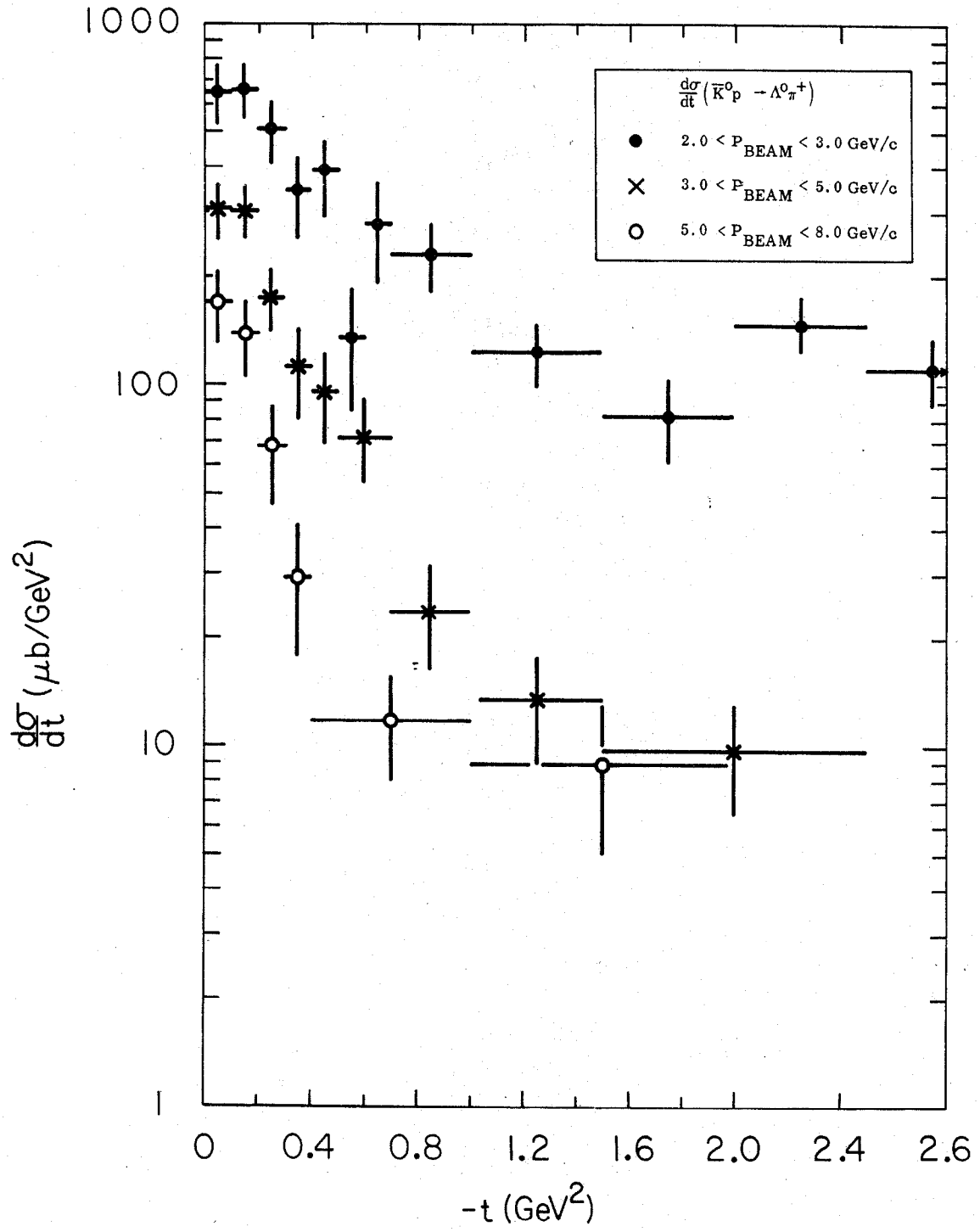
1000
100
10
1
$\frac{d\sigma}{dt}$ (μb/GeV^2)
$\frac{d\sigma}{dt}(\bar{K}^0 p \to \Lambda^0 \pi^+)$
2.0 < P_{BEAM} < 3.0 GeV/c
3.0 < P_{BEAM} < 5.0 GeV/c
5.0 < P_{BEAM} < 8.0 GeV/c
0
0.4
0.8
1.2
1.6
2.0
2.4
2.6
-t (GeV^2)

Fig. 13

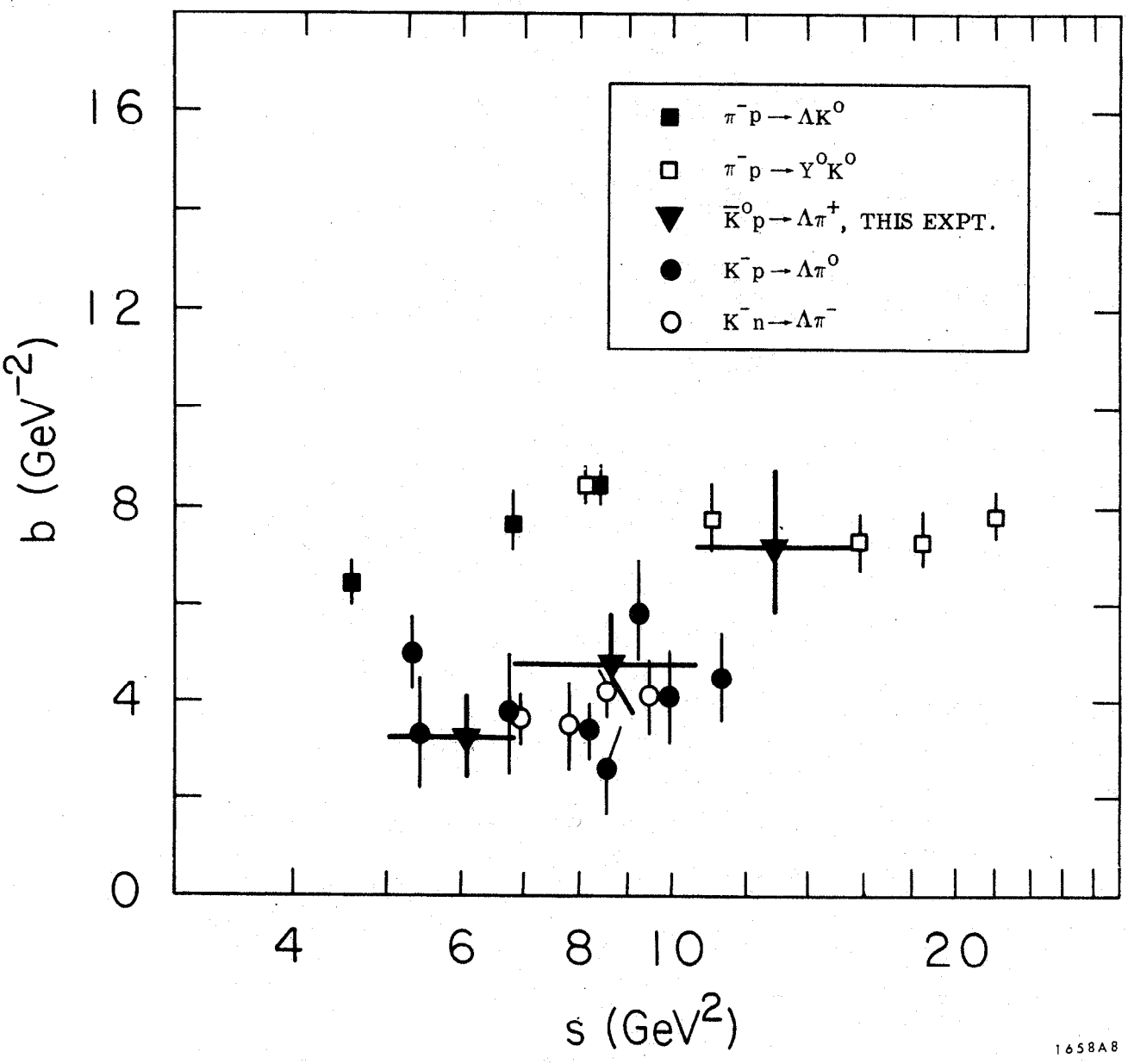
16
12
8
4
0
b (GeV^{-2})
4
6
8
10
20
s (GeV^2)
$\pi^- p \rightarrow \Lambda K^0$
$\pi^- p \rightarrow Y^0 K^0$
$\bar{K}^0 p \rightarrow \Lambda \pi^+$, THIS EXPT.
$K^- p \rightarrow \Lambda \pi^0$
$K^- n \rightarrow \Lambda \pi^-$
1658A8

Fig. 14

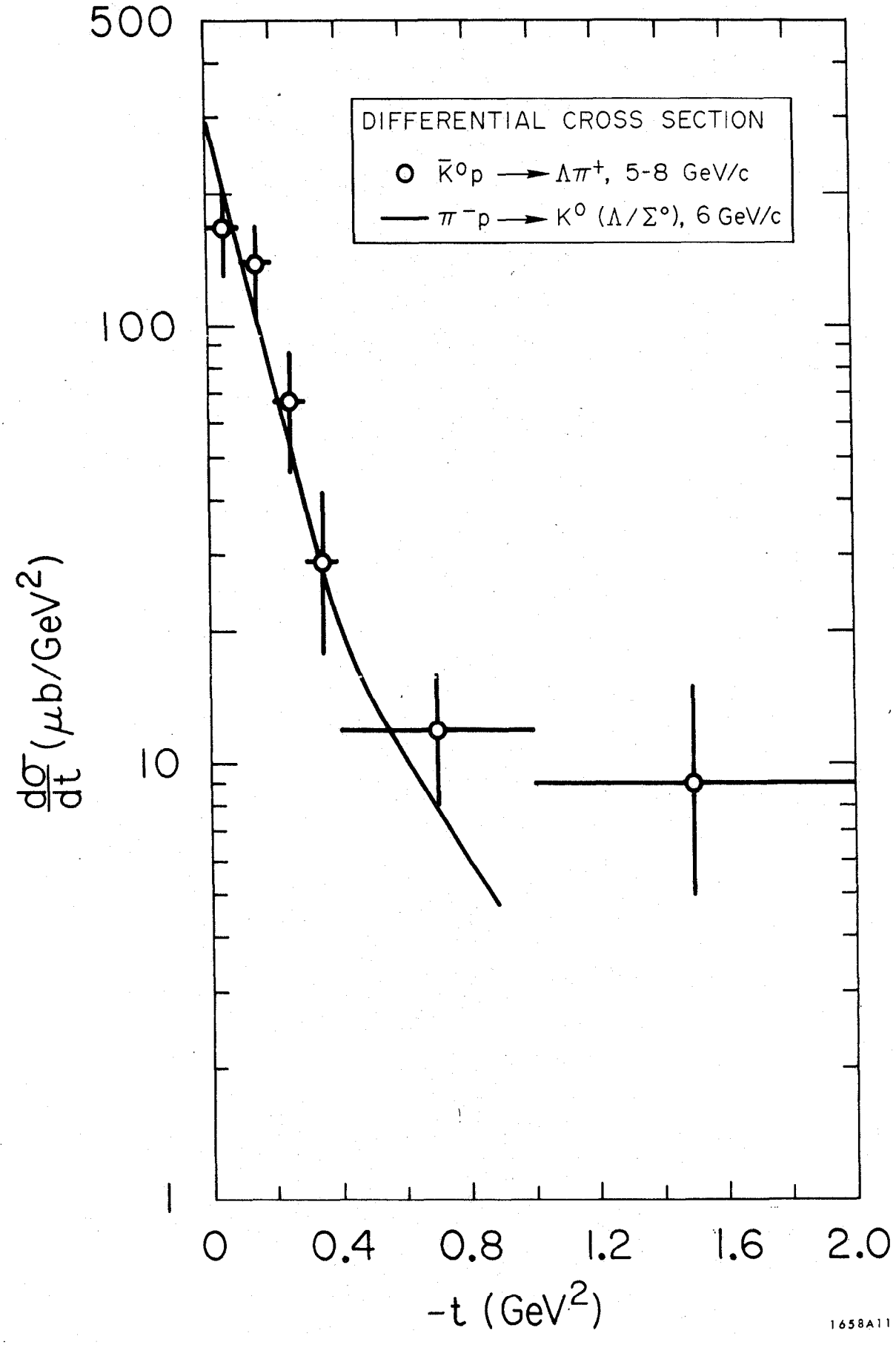
DIFFERENTIAL CROSS SECTION
$\bar{K}^0 p \longrightarrow \Lambda\pi^+$, 5-8 GeV/c
$\pi^- p \longrightarrow K^0 (\Lambda/\Sigma^0)$, 6 GeV/c
500
100
10
1
$\frac{d\sigma}{dt}$ (μb/GeV^2)
0
0.4
0.8
1.2
1.6
2.0
$-t$ (GeV^2)
1658A11

Fig. 15

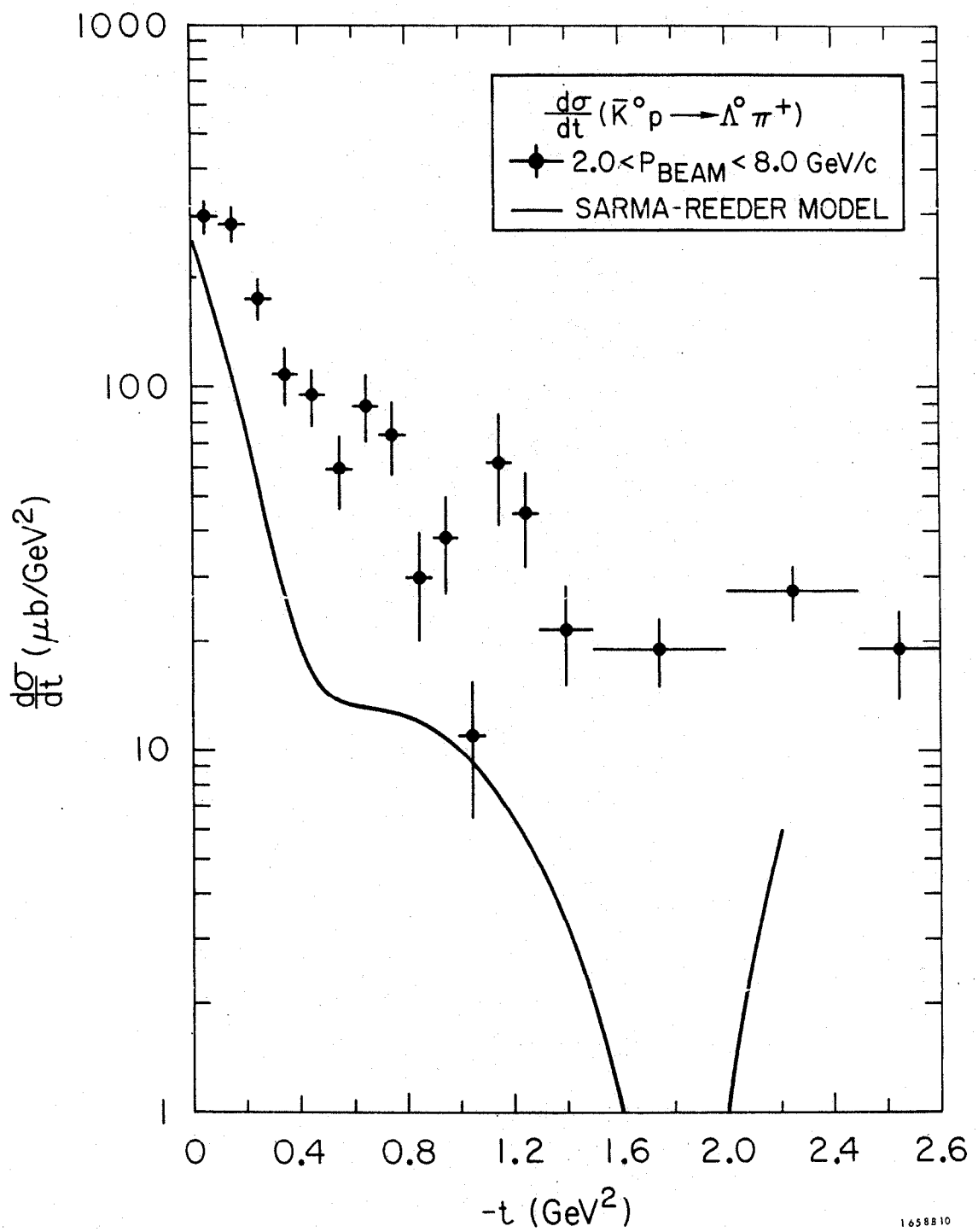
1000
100
10
1
$\frac{d\sigma}{dt}$ (μb/GeV^2)
$\frac{d\sigma}{dt}(\bar{K}^\circ p \rightarrow \Lambda^\circ \pi^+)$
2.0<P_{BEAM}<8.0 GeV/c
SARMA-REEDER MODEL
0
0.4
0.8
1.2
1.6
2.0
2.4
2.6
-t (GeV^2)
165B10

Fig. 16

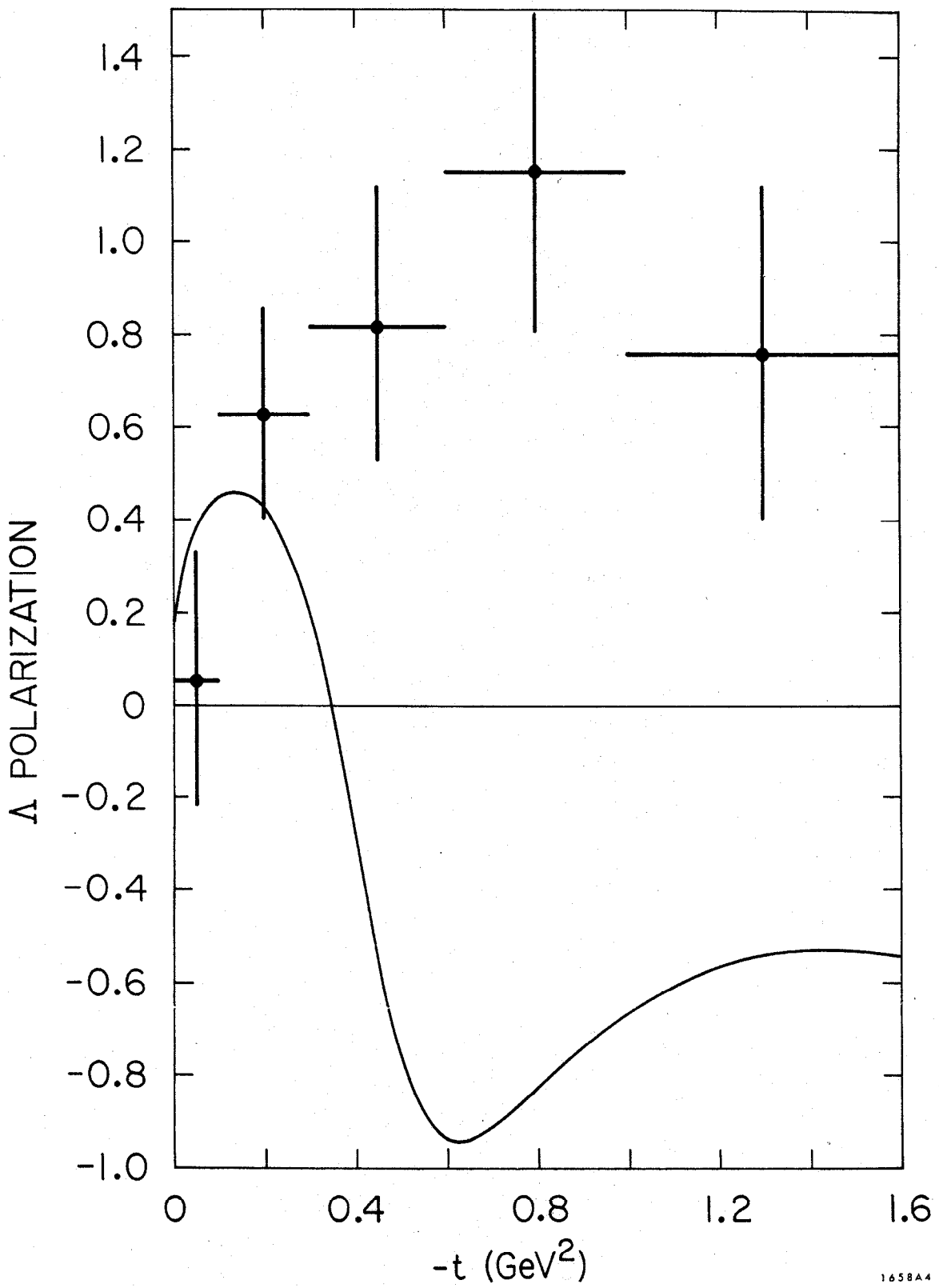
1.4
1.2
1.0
0.8
0.6
0.4
0.2
0
-0.2
-0.4
-0.6
-0.8
-1.0
Λ POLARIZATION
0
0.4
0.8
1.2
1.6
-t (GeV²)
1658A4

Fig. 17

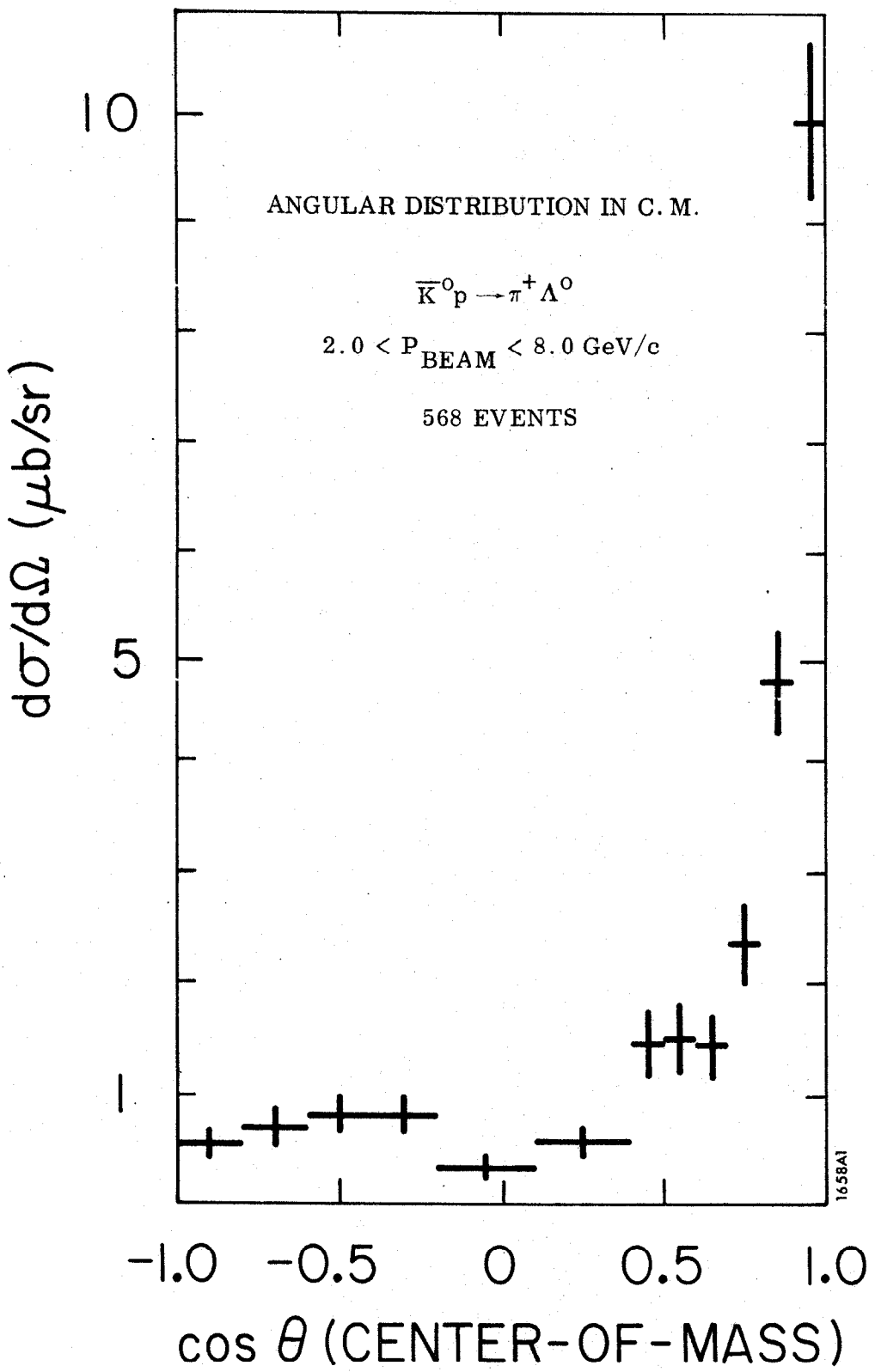
ANGULAR DISTRIBUTION IN C. M.
$\overline{K}^0 p \rightarrow \pi^+ \Lambda^0$
$2.0 < P_{BEAM} < 8.0$ GeV/c
568 EVENTS
10
5
1
$d\sigma/d\Omega$ (μb/sr)
-1.0
-0.5
0
0.5
1.0
cos θ (CENTER-OF-MASS)
1658A1

Fig. 18

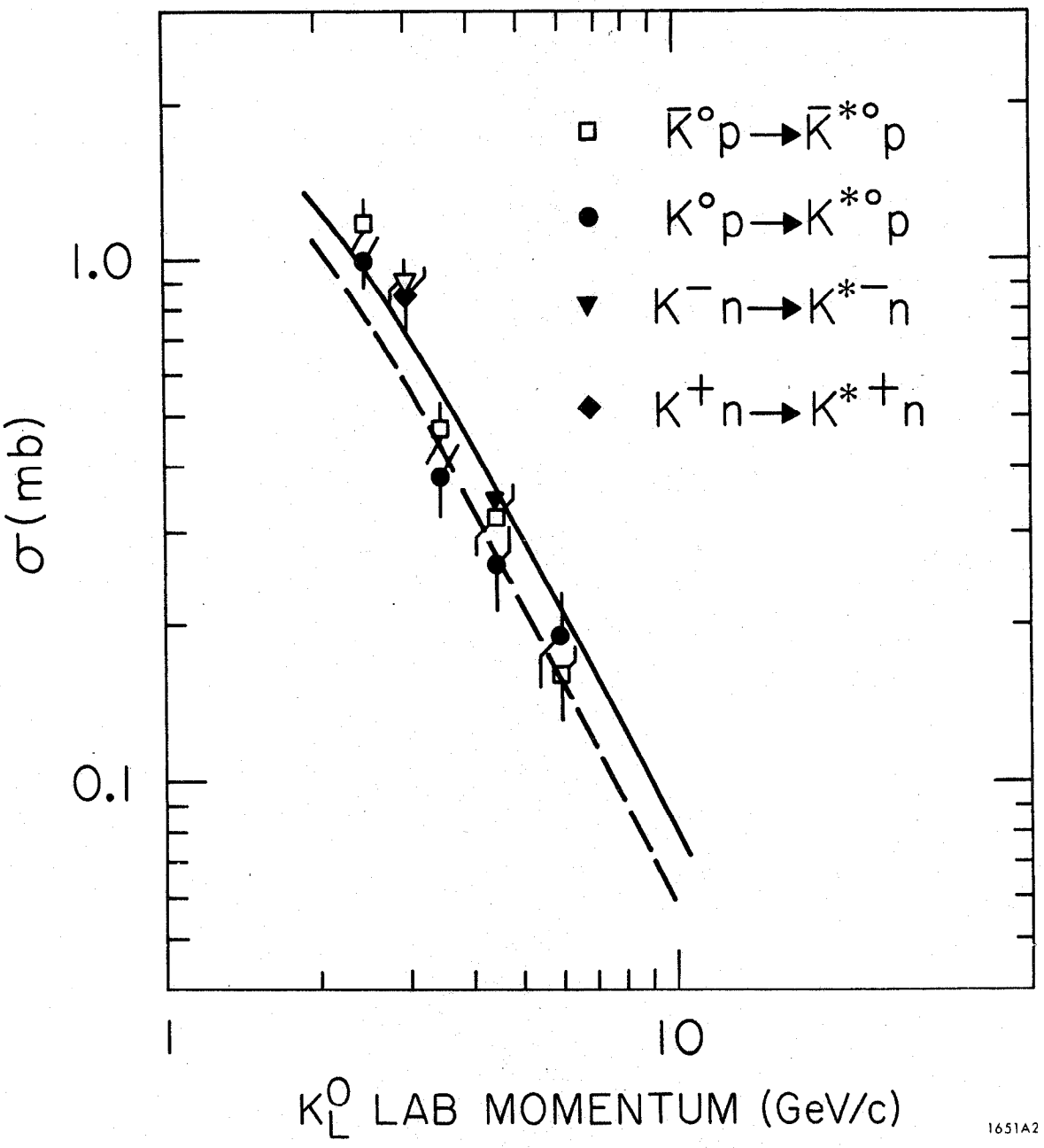
$\bar{K}^0 p \rightarrow \bar{K}^{*0} p$
$K^0 p \rightarrow K^{*0} p$
$K^- n \rightarrow K^{*-} n$
$K^+ n \rightarrow K^{*+} n$
1.0
0.1
σ(mb)
1
10
K_L^0 LAB MOMENTUM (GeV/c)
1651A2

Fig. 19

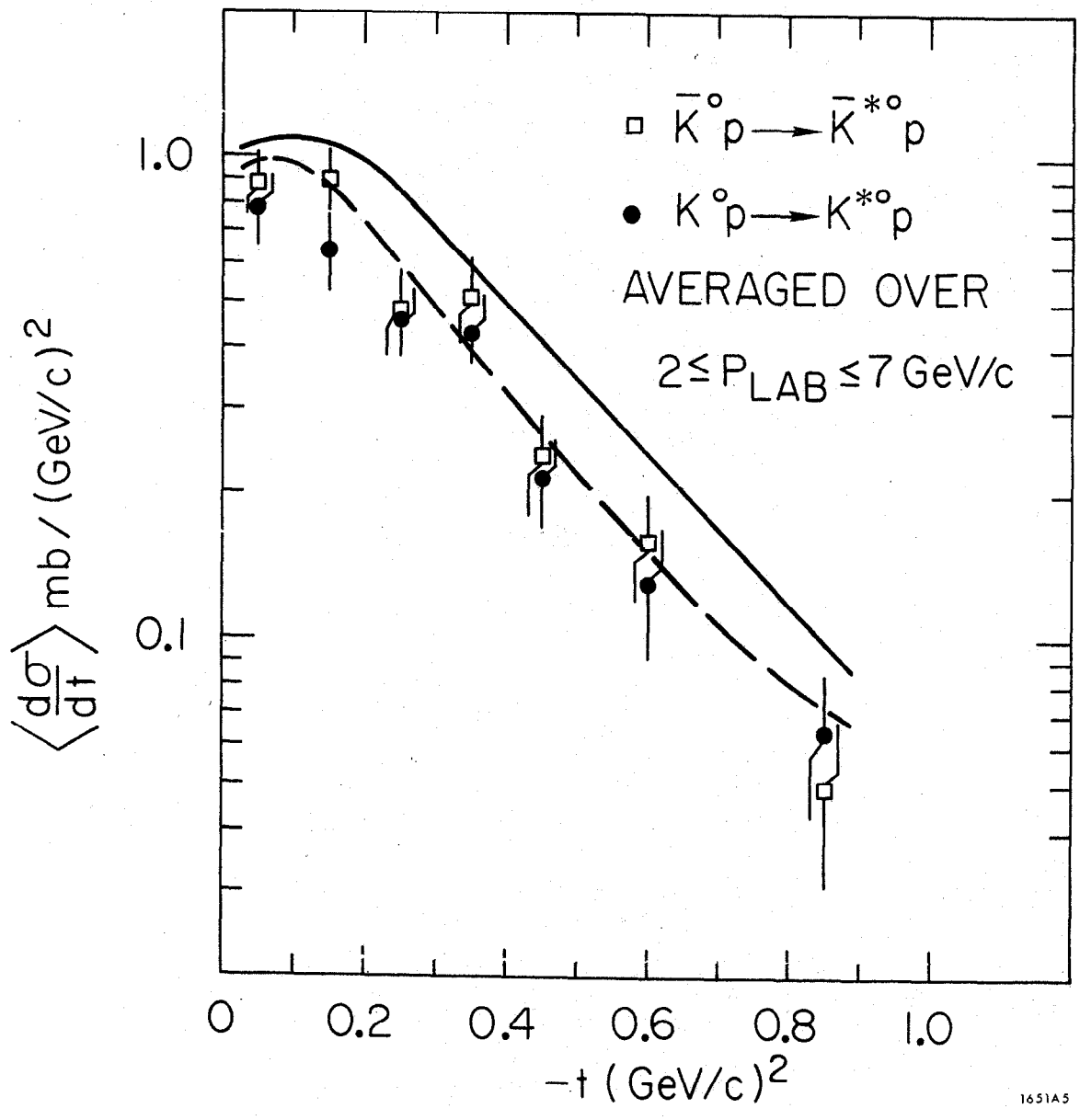
$\bar{K}^0 p \rightarrow \bar{K}^{*0} p$
$K^0 p \rightarrow K^{*0} p$
AVERAGED OVER
$2 \leq P_{LAB} \leq 7$ GeV/c
$\left\langle \frac{d\sigma}{dt} \right\rangle$ mb/(GeV/c)^2
1.0
0.1
0
0.2
0.4
0.6
0.8
1.0
$-t$ (GeV/c)^2
1651A5

Fig. 20

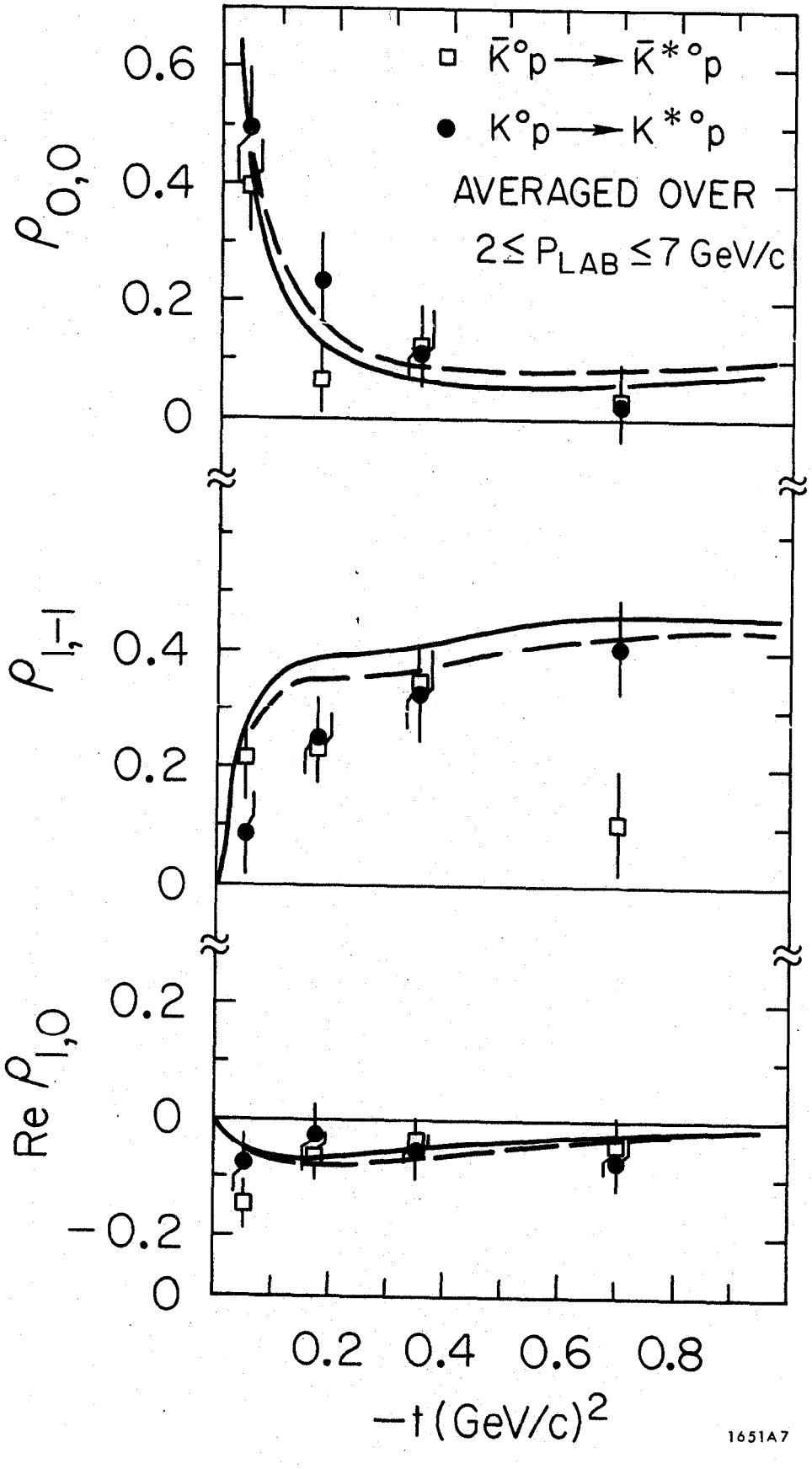
$\bar{K}^0p \rightarrow \bar{K}^{*0}p$
$K^0p \rightarrow K^{*0}p$
AVERAGED OVER
$2 \leq P_{LAB} \leq 7$ GeV/c
$\rho_{0,0}$
$\rho_{1,-1}$
Re $\rho_{1,0}$
0.6
0.4
0.2
0
0.4
0.2
0
0.2
0
−0.2
0
0.2 0.4 0.6 0.8
$-t\,(\mathrm{GeV/c})^2$
1651A7

Fig. 21

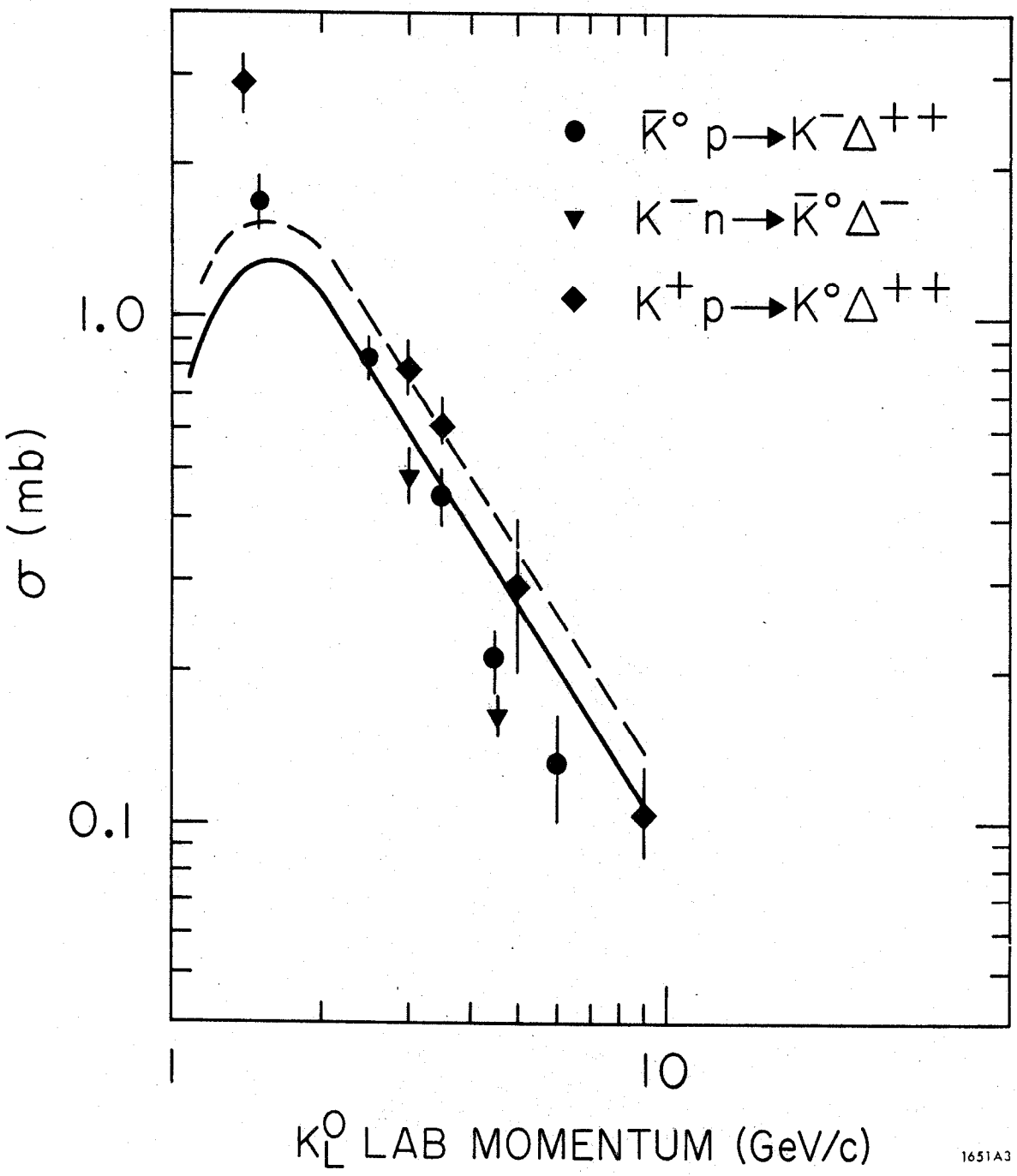
$\bar{K}^0 p \rightarrow K^- \Delta^{++}$
$K^- n \rightarrow \bar{K}^0 \Delta^-$
$K^+ p \rightarrow K^0 \Delta^{++}$
1.0
0.1
σ (mb)
1
10
K_L^0 LAB MOMENTUM (GeV/c)
1651A3

Fig. 22

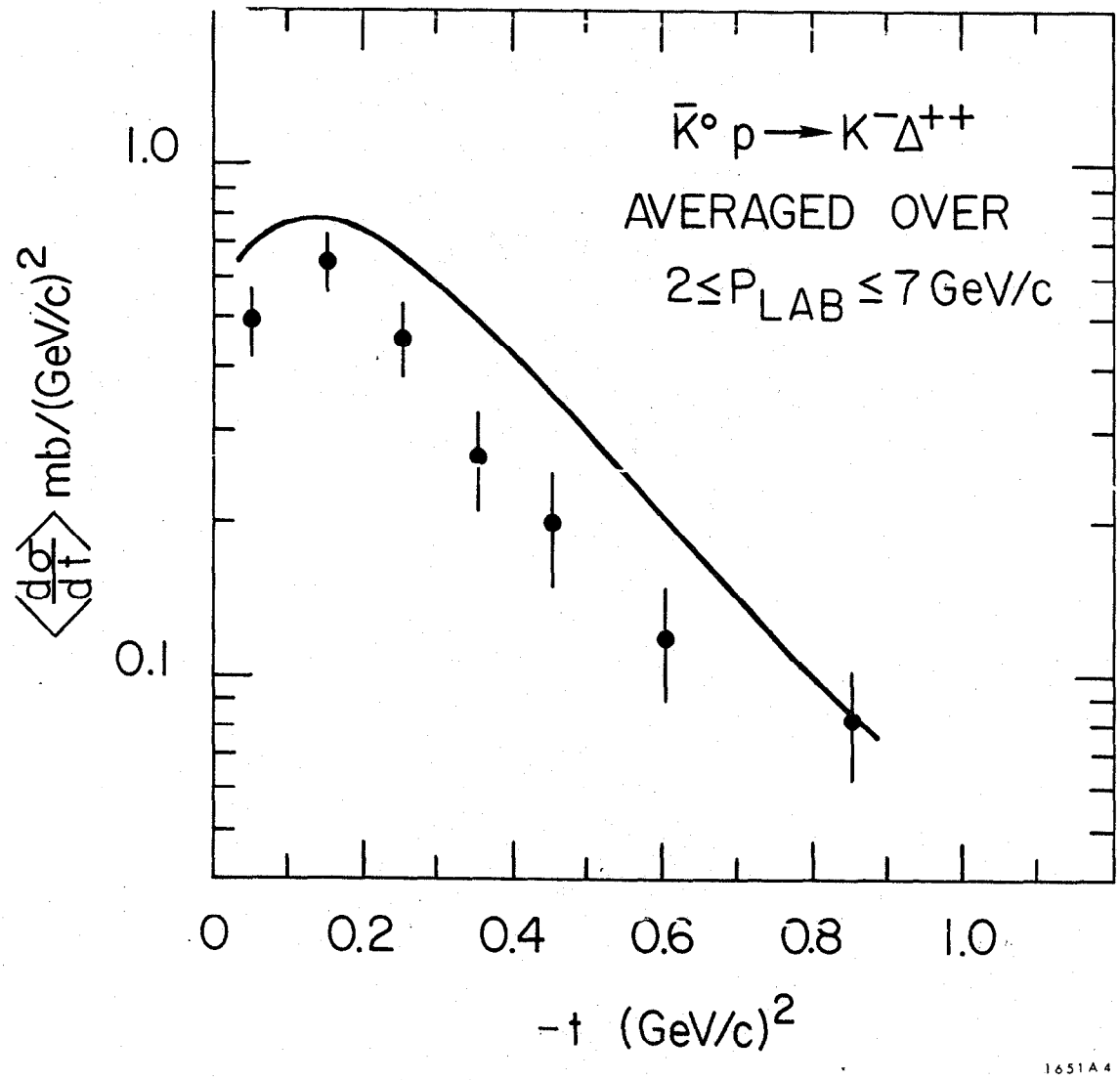
$\bar{K}^0 p \rightarrow K^- \Delta^{++}$
AVERAGED OVER
$2 \leq P_{LAB} \leq 7$ GeV/c
$\left\langle \frac{d\sigma}{dt} \right\rangle$ mb/(GeV/c)^2
1.0
0.1
0
0.2
0.4
0.6
0.8
1.0
$-t$ (GeV/c)^2
1651A4

Fig. 23

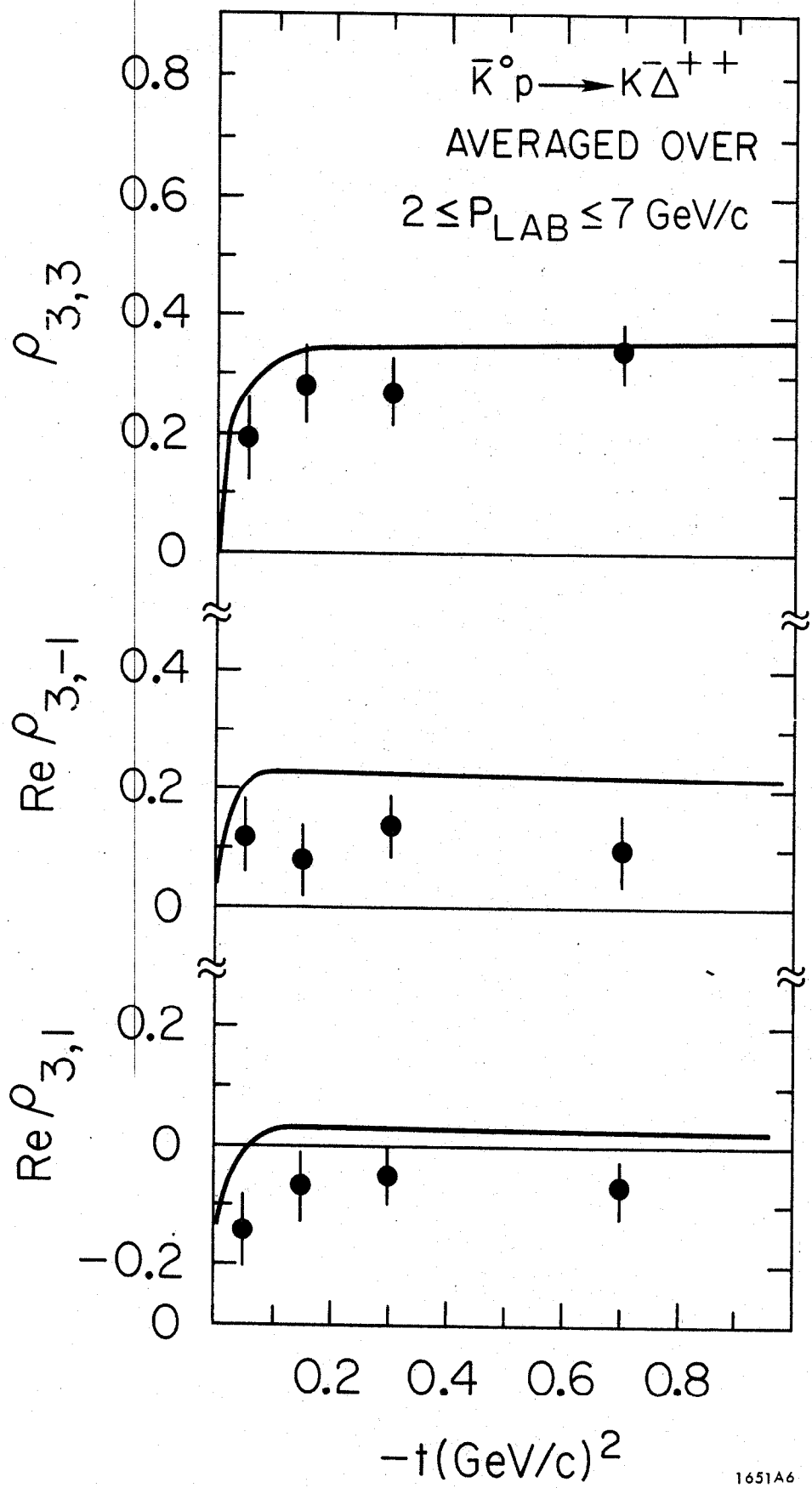
$\bar{K}^0 p \rightarrow K^- \Delta^{++}$
AVERAGED OVER
$2 \leq P_{LAB} \leq 7$ GeV/c
$\rho_{3,3}$
$\mathrm{Re}\,\rho_{3,-1}$
$\mathrm{Re}\,\rho_{3,1}$
0.8
0.6
0.4
0.2
0
0.4
0.2
0
0.2
0
−0.2
0
0.2
0.4
0.6
0.8
$-t(\mathrm{GeV/c})^2$
1651A6

Fig. 24

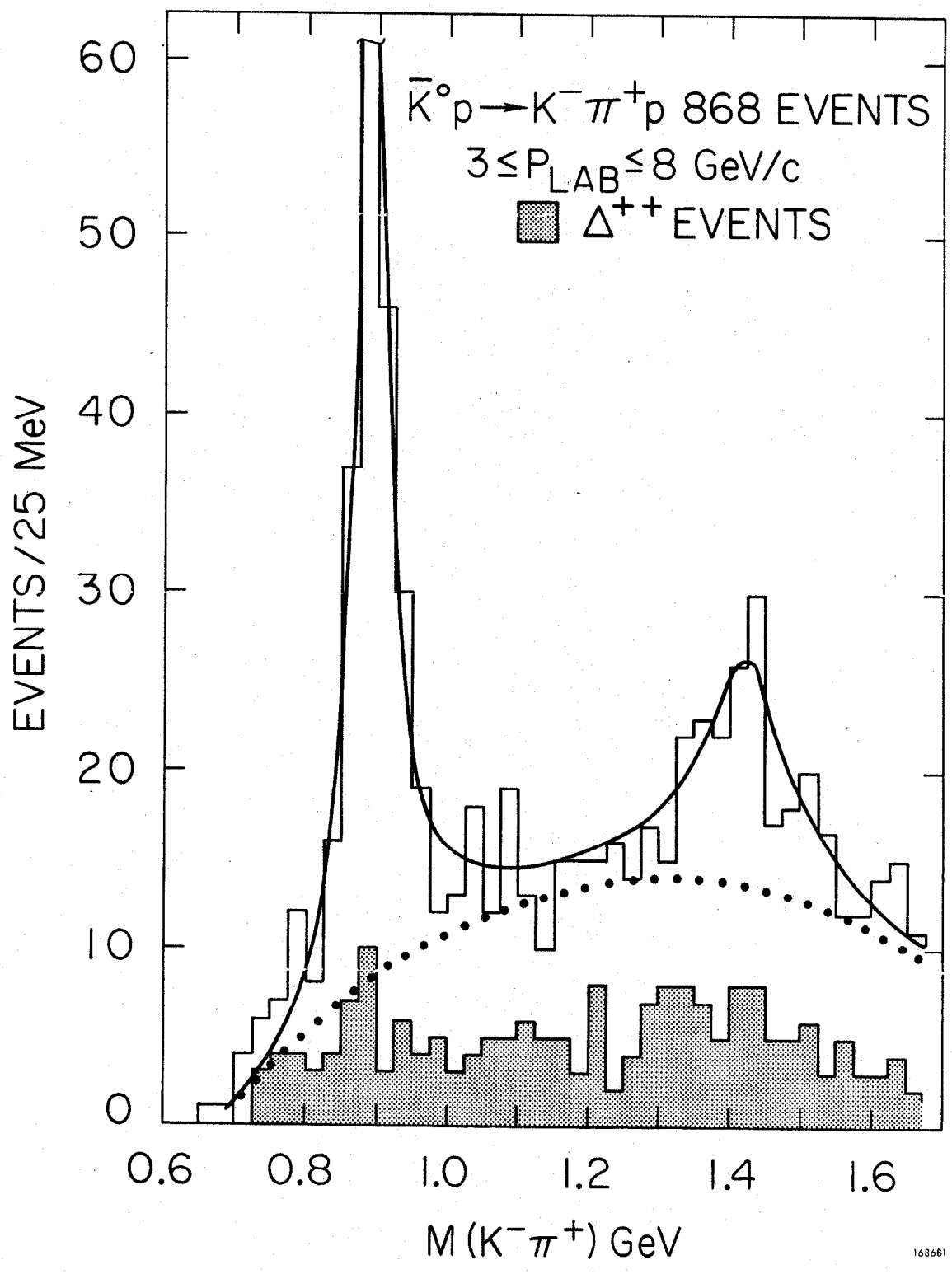
$\bar{K}^0 p \rightarrow K^- \pi^+ p$ 868 EVENTS
$3 \leq P_{LAB} \leq 8$ GeV/c
Δ^{++} EVENTS
EVENTS/25 MeV
0
10
20
30
40
50
60
0.6
0.8
1.0
1.2
1.4
1.6
M ($K^- \pi^+$) GeV
168681

Fig. 25

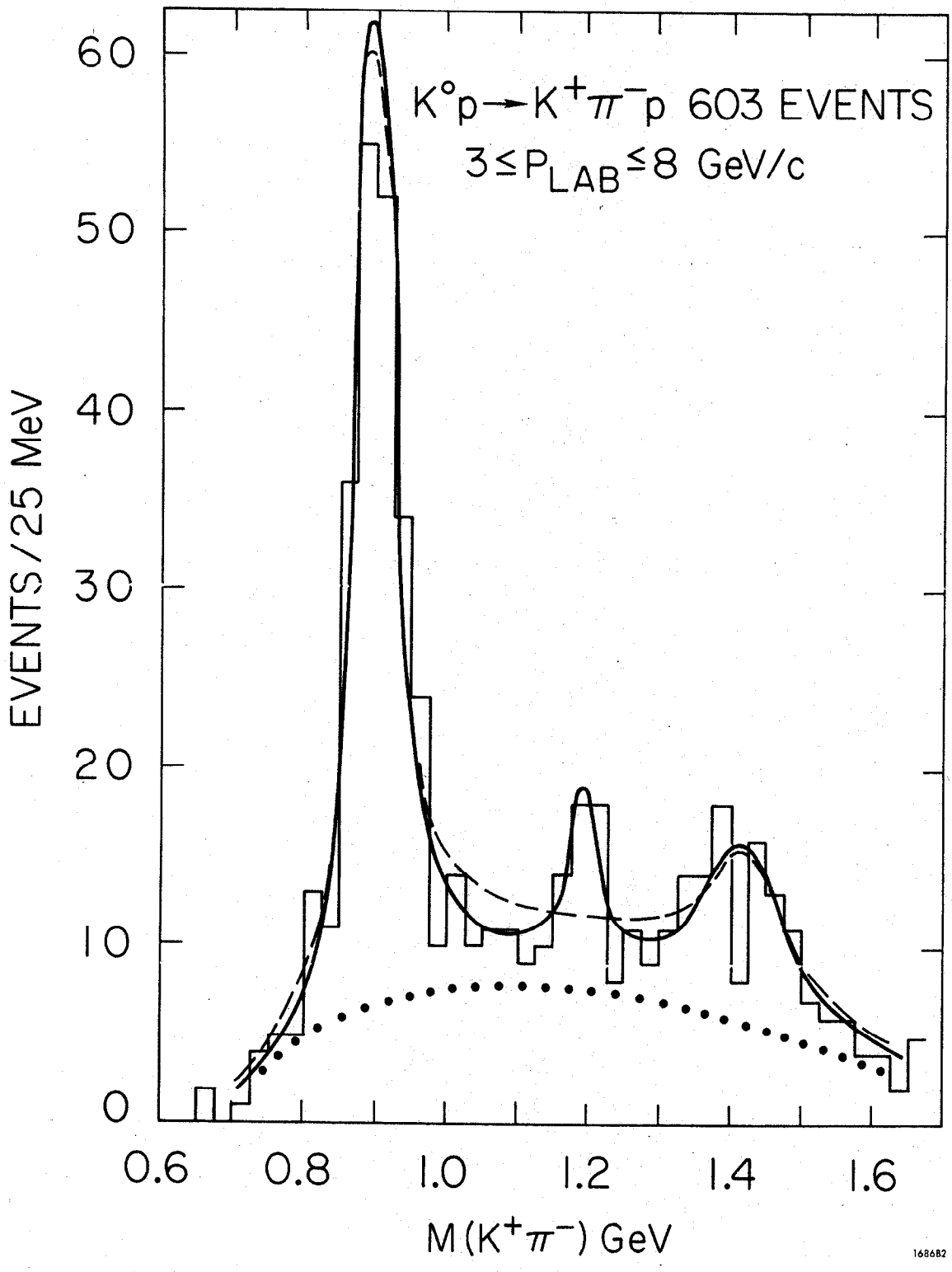
$K^0p \rightarrow K^+\pi^-p$ 603 EVENTS
$3 \leq P_{LAB} \leq 8$ GeV/c
EVENTS/25 MeV
0
10
20
30
40
50
60
0.6
0.8
1.0
1.2
1.4
1.6
$M(K^+\pi^-)$ GeV
168682

Fig. 26